JOURNAL OF GEOPHYSICAL RESEARCH, VOL. 99, NO. B9, PAGES 18,175–18,201, SEPTEMBER 10, 1994

Tertiary structural evolution of the Gangdese thrust system, southeastern Tibet

An Yin,[1] T. Mark Harrison,[1] F.J. Ryerson,[2] Chen Wenji,[3] W.S.F. Kidd,[4] and Peter Copeland[5]

Abstract. Structural and thermochronological investigations of southern Tibet (Xizang) suggest that intracontinental thrusting has been the dominant cause for formation of thickened crust in the southernmost Tibetan plateau since late Oligocene. Two thrust systems are documented in this study: the north dipping Gangdese system (GTS) and the younger south dipping Renbu-Zedong system (RZT). West of Lhasa, the Gangdese thrust juxtaposes the Late Cretaceous forearc basin deposits of the Lhasa Block (the Xigaze Group) over the Tethyan sedimentary rocks of the Indian plate, whereas east of Lhasa, the fault juxtaposes the Late Cretaceous-Eocene, Andean-type arc (the Gangdese batholith) over Tethyan sedimentary rocks. Near Zedong, 150 km southeast of Lhasa, the Gangdese thrust is marked by a >200-m-thick mylonitic shear zone that consists of deformed granite and metasedimentary rocks. A major south dipping backthrust in the hanging wall of the Gangdese thrust puts the Xigaze Group over Tertiary conglomerates and the Gangdese plutonics north of Xigaze and west of Lhasa. A lower age bound for the Gangdese thrust of 18.3±0.5 Ma is given by crosscutting relationships. The timing of slip on the Gangdese thrust is estimated to be 27-23 Ma from $^{40}Ar/^{39}Ar$ thermochronology, and a displacement of at least 46±9 km is indicated near Zedong. The age of the Gangdese thrust (GT) is consistent with an upper age limit of ~24 Ma for the initiation of movement on the Main Central thrust. In places, the younger Renbu-Zedong fault is thrust over the trace of the GT, obscuring its exposure. The RZT appears to have been active at circa 18 Ma but had ceased movement by 8±1 Ma. The suture between India and Asia has been complexly modified by development of the GTS, RZT, and, locally, strike-slip and normal fault systems.

Introduction

Various strain accommodation mechanisms have been attributed to the Indo-Eurasia collision during the Tertiary, including strike-slip faulting [*Tapponnier et al.*, 1982], thrusting [*Argand*, 1924; *Powell and Conaghan*, 1973; *Dewey and Burke*, 1973; *Dewey et al.*, 1989], and a combination of both that vary in space and time during the protracted collision [*Harrison et al.*, 1992a]. It has long been appreciated that at least a portion of the Tertiary convergence has been accommodated by major intra-continental thrusts in the Himalaya [*LeFort*, 1986; *Mattauer*, 1986; *Bouchez and Pêcher*, 1981]. Although syncollisional thrusts have been mapped within Tethyan strata on the northern flank of the Himalaya [*Wang et al.*, 1983; *Burg*, 1983], no Tertiary, crustal-scale thrusts have been reported from the Lhasa Block. However, geologic relationships, in particular the juxtaposition of Tethyan continental margin deposits against Andean-type plutonic rocks (the Gangdese batholith), suggest that a south directed, intracontinental thrust system may have been active in southern Tibet subsequent to collision [e.g., *Searle et al.*, 1987]. In light of thermochronological results from southeastern Tibet that appear to require such a structure, we previously proposed [*Harrison et al.*, 1992a] the existence of a fault we termed the Gangdese thrust system (GTS). We present here the results of field observations conducted during the summer of 1992, together with further thermochronological analyses, that confirm our predictions regarding the GTS and constrain its timing, structural style, and kinematic history. Implications of the GTS for the Indo-Asia collision are discussed and a tectonic interpretation for the Tertiary evolution of the southern Tibetan plateau and the Higher (= Greater) Himalaya is proposed.

Geologic Setting

Major tectonic elements in southern Tibet (Plate 1) consist of a pre-early Tertiary thrust belt along the northern margin of the Lhasa Block (the accreted continental block bounded on the south and north by the Indus-Tsangpo and Banggong sutures, respectively) [*Allegre et al.*, 1984; *Dewey et al.*, 1988], an Andean-type Mesozoic to early Tertiary igneous belt (the Gangdese batholith and Linzizong volcanics), a late Cretaceous-early Tertiary forearc basin (the Xigaze Group), and the ophiolitic Indus-Tsangpo suture zone (Plate 1, inset) that separates rocks in the Lhasa Block from rocks of Indian affinity. The presence of the Gangdese batholith and the

[1]Department of Earth and Space Sciences and Institute of Geophysics and Planetary Physics, University of California, Los Angeles.

[2]Institute of Geophysics and Planetary Physics, Lawrence Livermore National Laboratory, Livermore, California.

[3]Institute of Geology, State Seismological Bureau, Beijing.

[4]Department of Geological Sciences, State University of New York at Albany.

[5]Department of Geosciences, University of Houston, Houston, Texas.

Paper number 94JB00504.
0148-0227/94/94JB-00504$05.00

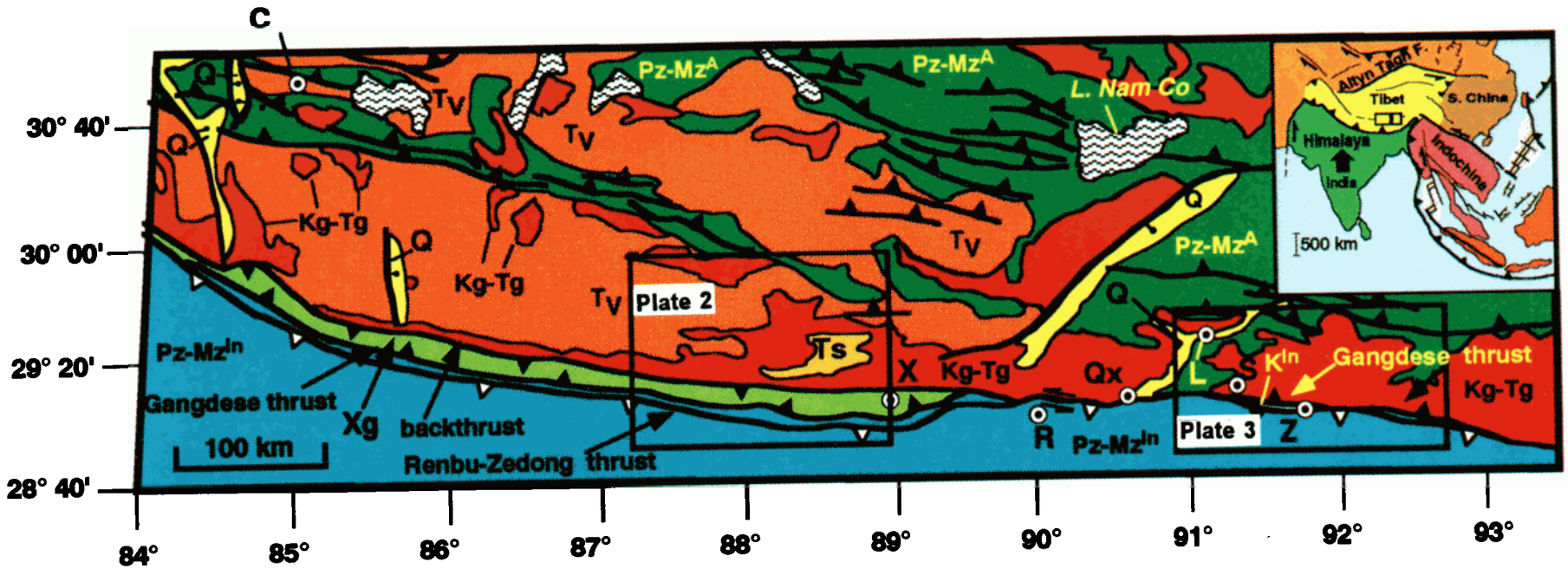

Plate 1. Tectonic map of southern Tibet, simplified from *Liu et al.* [1988], and locally modified on the basis of our field observations. C, Chouqin; L, Lhasa; Qx, Quxu; S, Samye; R, Renbu; X, Xigaze; Q, Quaternary sediments; Z, Zedong; Pz-Mz^{A}, Paleozoic and Mesozoic sedimentary rocks of the Lhasa Block in the Asian plate; T_s, Tertiary sedimentary rocks; T_v, Tertiary volcanic rocks of the Linzizhong Formation; Kg-Tg, Cretaceous to early Tertiary granites of the Gangdese ingeous belt; Pz-Mz^{In}, Paleozoic and Mesozoic sedimentary rocks of the Indian plate (= Tethyan sedimentary rocks); K^{In}, Cretaceous metasedimentary rocks of the Indian plate; X_g, Xigaze Group. Thrust fault with open triangles represents the trace of the Renbu-Zedong thrust (RZT). Lakes are indicated by the wavy pattern.

forearc sequence of the Xigaze Group suggests that convergence between the Indian and Eurasian plates prior to the continental collision was accommodated by a north dipping subduction zone beneath southern Asia. Field observations show, however, that the Indus-Tsangpo suture zone is south dipping near Gongga (Plate 3a) [e.g., *Allegre et al.*, 1984], suggesting that the suture was deformed subsequent to closure of the ocean(s) that once separated India from Asia. In this paper we argue that this south dipping contact represents a Neogene north directed thrust (the Renbu-Zedong fault) that postdates the Gangdese thrust along the southern edge of the Lhasa Block.

The Gangdese batholith is broadly characterized by exposure of Cretaceous to Tertiary volcanic and hypabyssal rocks west of the longitude of Renbu, and age-equivalent plutonic rocks east of Renbu (Plate 1). This map relation indicates differential unroofing along strike: the structural level of pluton exposure near Lhasa is between 10 to 15 km as indicated by thermochronometry and barometry [*Copeland et al.*, 1987, 1994], whereas the widespread preservation of volcanic rocks in this belt suggests much less denudation west of Renbu. Spatially corresponding to the preservation of volcanic cover in the Gangdese Shan is the appearance, to the south, of the Xigaze Group (Plate 1). The tectonic basis of this relationship has been investigated in light of the structural and thermochronological studies. We propose that the distribution of these rock units in southern Tibet are best explained by a variation in structural style and magnitude of displacement along the GTS. The present Indus-Tsangpo suture is not the trace of a single fault contact marking the locus of oceanic closure between India and Asia. Rather, it is a composite structural feature resulting from multiphase deformation including both dip-slip and strike-slip faulting since the late Oligocene.

Structural Geology

Various structural features have been observed in the southern Tibetan plateau during our field study, including thrusts, strike-slip faults, normal faults, folds and foliations. Tectonic positions, structural style, and timing of formation for those related to the Indo-Asia collision are described below.

Thrust Systems

A north dipping thrust is well exposed in the Zedong and Xigaze areas (Plates 1-3). In the Xigaze area (Plate 2*a*), the north dipping fault juxtaposes the Xigaze Group over Tethyan strata of the Indian plate. Rocks directly below the fault are extensively fractured and sheared. In contrast, south verging mesoscopic folds are the dominant structures in the Xigaze Group in the hanging wall. Dominant east-west trending and south verging folds directly above the fault suggest that it is south directed (Plate 4a). Although some of the hanging wall deformation could be subduction related, a substantial portion of it must postdate collision as the overlying Eocene (?) Qiuwu conglomerate [*Wang et al.*, 1983] is also intensely folded. In the Zedong area (Plate 3a), the north dipping thrust juxtaposes the Gangdese plutonic rocks and metasedimentary rocks over ~1-km-thick Tertiary(?) conglomerates and Tethyan sediments (Plate 4b). Clasts of the Tertiary(?) conglomerates are predominantly marble and granite that were likely derived from the hanging wall metasedimentary country rocks intruded by the Gangdese batholith. The thrust near Zedong is defined by a well-exposed >200-m-thick mylonitic shear zone dipping at between 25°-35° to the north and consisting of granitic rocks and marble (Plate 4c). Mesoscopic structures including south verging folds (Plate 4d), tension gashes, and asymmetric boudinage structures (Plate 4d) are abundant in the mylonitic shear zone and suggest a top-to-the-south sense of shear, consistent with the field relationship. Microscopic examination of kinematic indicators in the mylonitic rocks likewise suggests the same sense of shear. We propose below that the south-directed faults near Zedong and Xigaze are both manifestations of the Gangdese thrust system that was variably active during the late Oligocene to Miocene.

Based on Chinese mapping [*Wang et al.*, 1983] and our own observations, the structural style in the hanging wall of these north dipping thrusts appears to vary along strike. For example, west of Renbu, the Gangdese thrust (GT) may be manifested as two opposed thrust faults (a "pop-up" structure); a north dipping thrust bounding the southern limit of the Xigaze Group and a south dipping thrust juxtaposing these forearc sediments against Tertiary conglomeratic sandstones and Gangdese plutonic rocks. As Chinese mapping indicates that this latter feature merges with the GT near Renbu, we interpret it to be a backthrust of the GT (Plates 1 and 2). This relationship suggests that the two thrusts that bound the Xigaze rocks were coeval (Plate 2). Structures in the hanging wall of this backthrust are characterized by the development of north directed imbricate and duplex thrust systems (Plate 4e); this structural style differs from the widespread asymmetric folds in the Xigaze Group immediately above the GT to the south. The backthrust is cut by a series of north-south trending andesitic dikes. Near Zedong, 200 km east of Renbu, the GTS is characterized by a single major thrust (Plates 1 and 3). Spatially corresponding to this change in style of deformation east of Renbu is the absence of the Xigaze Group either in the hanging wall or footwall of the GT.

There are three possible explanations for the absence of the Xigaze Group rocks east of Renbu: erosion, removal by strike-slip faulting, or thrusting beneath the Gangdese fault. For Xigaze Group rocks to have been eroded away above the GT requires that the Gangdese plutonic rocks to predate the forearc sediments, since nowhere is an intrusive relationship observed. However, the Xigaze Group is largely Cretaceous while Gangdese granodiorites are as young as Eocene making the exposed granitoids in the Zedong area unlikely candidates as basement of the Xigaze Group. At Quxu, 60 km southwest of Lhasa (Plate 1), another location where Tethyan strata directly abut the Lhasa Block, the granitoids are firmly dated at 41±1 Ma [*Schärer et al.*, 1986]. Although it is possible that much of the suture zone could have been shifted to the east by strike-slip faulting, Xigaze Group rocks have not been identified in eastern Tibet or Yunnan. Furthermore, the Xigaze Group also disappears west of Mt. Kailas [*Harrison et al.*, 1993a] where plutonic rocks are widely exposed, making it difficult to understand how right-lateral strike-slip faulting could remove both the western and eastern portions of the forearc sediments but leave the central region exposed. This conjecture also does not explain the close relationship between the Xigaze Group and adjacent volcanic rocks of the Gangdese batholith where the forearc is preserved. Thus we conclude that, east of Renbu, at least the approximate present width of the Xigaze Group (~20 km) was thrust beneath the Gangdese batholith. Because the Xigaze and Eocene (?) Qiuwu strata have been substantially shortened [*Wang et al.*, 1983], at least in part since the collision began, the amount of displacement could be significantly greater. If we consider that 10-15 km of crust has been eroded away from much of the Gangdese batholith east of Renbu as a consequence of late Oligocene-Early Miocene thickening [*Copeland et al.*, 1987, 1994; *Harrison et al.*, 1992a] along a thrust dipping 30±5°, an additional 17-35 km of slip along the GT is indicated. Thus we estimate a minimum displacement on the thrust of 46±9 km.

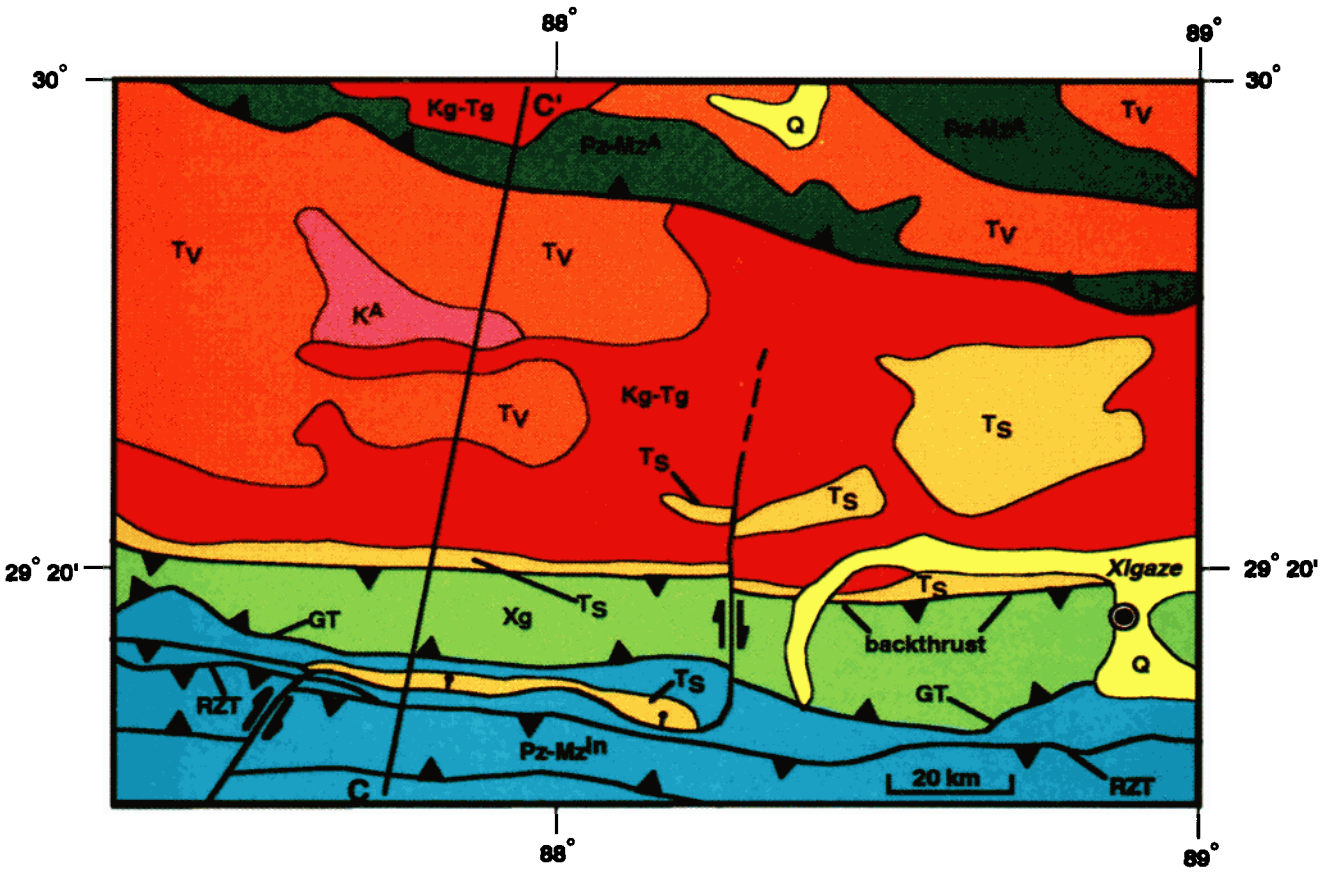

(a)

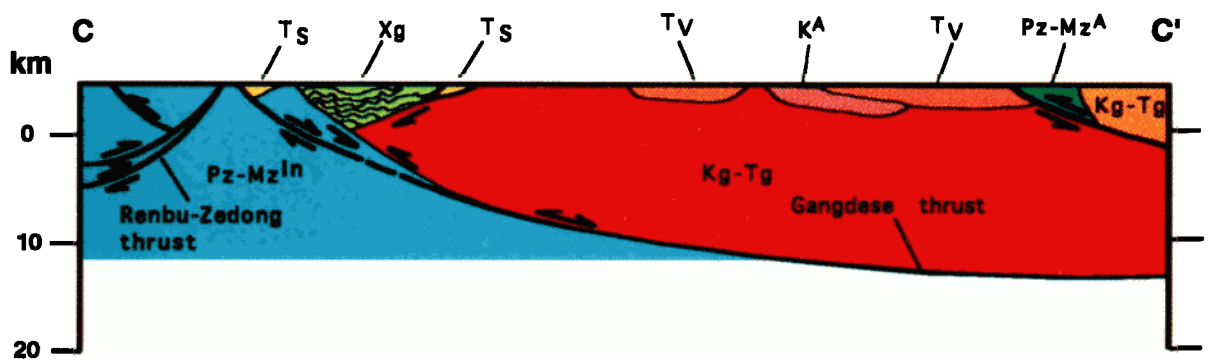

(b)

Plate 2. (a) Geologic map of the Xigaze area, modified from *Wang et al.* [1983] based on our field observations. Q, Quaternary sediments; T_S, Tertiary sedimentary rocks; T_V, early Tertiary volcanic rocks of the Linzizhong Formation; Kg-Tg, Cretaceous to early Tertiary granites of the Gangdese batholith; K^A, Cretaceous sedimentary of the Takena Formation; Pz-Mz^A, Paleozoic and Mesozoic sedimentary rocks of the Lhasa Block; X_g, Xigaze Group; Pz-Mz^{In}, Paleozoic and Mesozoic sedimentary rocks of the Indian plate. (b) Cross section C-C' showing structural style in the hanging wall of the Gangdese thrust near Xigaze.

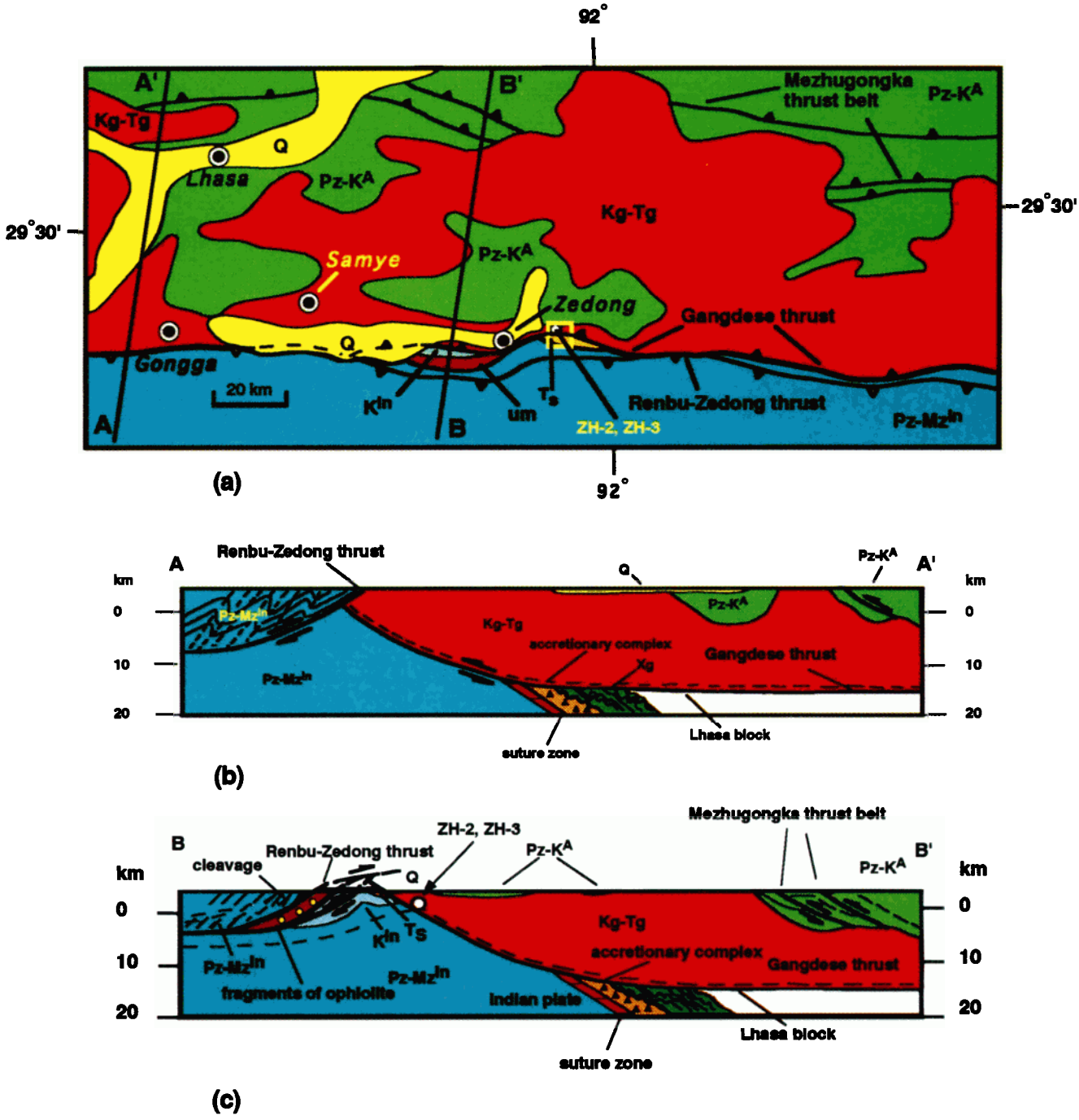

Plate 3. (a) Geologic map of the Zedong area, modified from *Wang et al.* [1983] and based on our field observations. Map symbols are the same as those used in Plates 1 and 2 (um, mafic/ultramafic complex). Cross sections (b) A-A' and (c) B-B' showing the relationship between the Renbu and Gangdese thrusts. Structural position of samples ZH-2b and ZH-3 are also shown.

The second major thrust investigated in this study is the south dipping Renbu-Zedong thrust (RZT). This fault was first mapped by Chinese geologists [*Wang et al.*, 1983] and later included in regional compilations of southern Tibetan geology [*Burg*, 1983; *Liu et al.*, 1988; *Kidd et al.*, 1988]. The RZT is clearly younger than the GT, because its hanging wall strata locally thrust over the trace of the GT, putting both the hanging wall and footwall rocks of the GT below its footwall. Near Gongga, south of Lhasa (Plates 1 and 2), the RZT juxtaposes very low-grade Tethyan metasedimentary rocks in its hanging wall and Cretaceous granitic and Paleozoic-Mesozoic metasedimentary rocks of the Lhasa Block in its footwall (Plate 5a). Note that without recognition of the GT, the field relationship near Gongga would suggest a normal fault relation for the Renbu-Zedong fault, because it juxtaposes upper structural level rocks (low-grade metasedimentary rocks) in the hanging wall over lower structural level rocks (granites and metamorphic rocks of greenschist to amphibolite facies) in the footwall. However, mesoscopic structures such as asymmetric folds and thrusts directly above the RZT indicate that the thrust is north directed. In addition, steeply south dipping cleavage is well

a

b

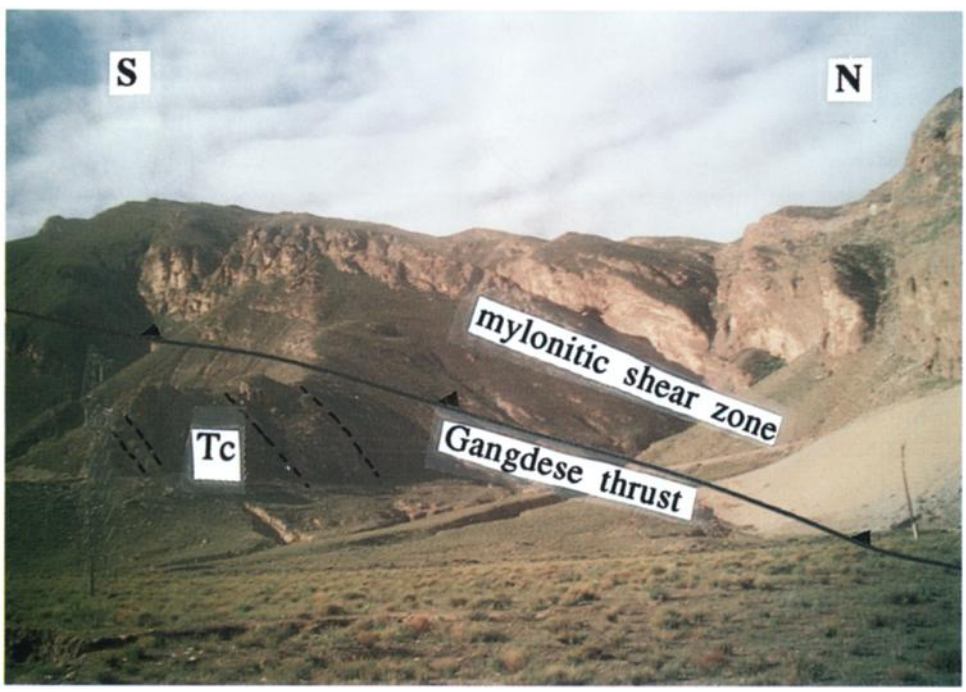

Plate 4. (a) South verging fold in the Xigaze Group in the hanging wall of the Gangdese thrust west of Xigaze; view to the northwest. The telephone poles in the foreground are about 7 m high. (b) The Gangdese thrust exposed near Zedong (see Plate 3a and Figure 1 for location). Cliff-forming unit is the mylonitic granite and marble in the hanging wall of the GT. Tc, Tertiary (?) conglomerates dipping steeply to the south in the footwall. (c) The mylonitic shear zone above the Gangdese thrust. (d) Minor asymmetric folds and boudinage structures in the mylonitic shear zone. (e) Duplex system in the hanging wall of the backthrust system northwest of Xigaze.

c

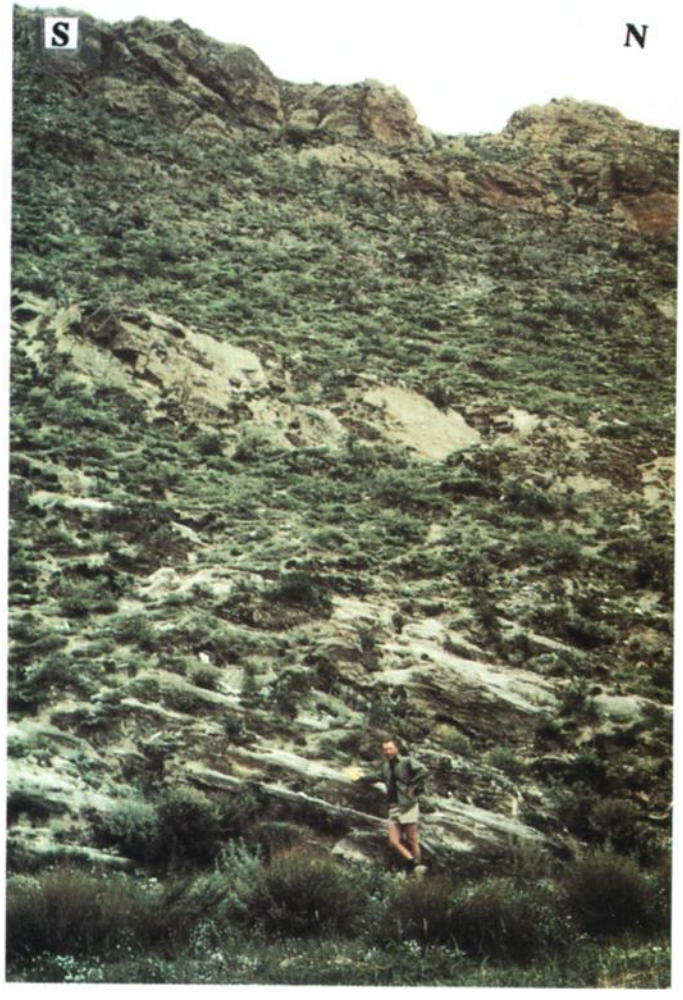

d

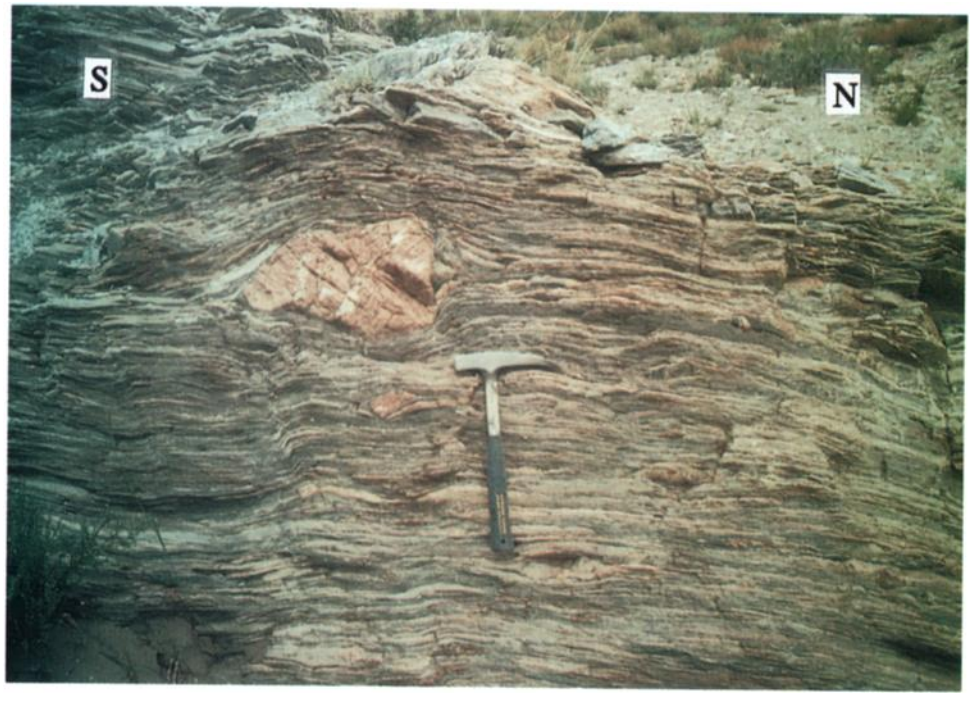

Plate 4. (continued)

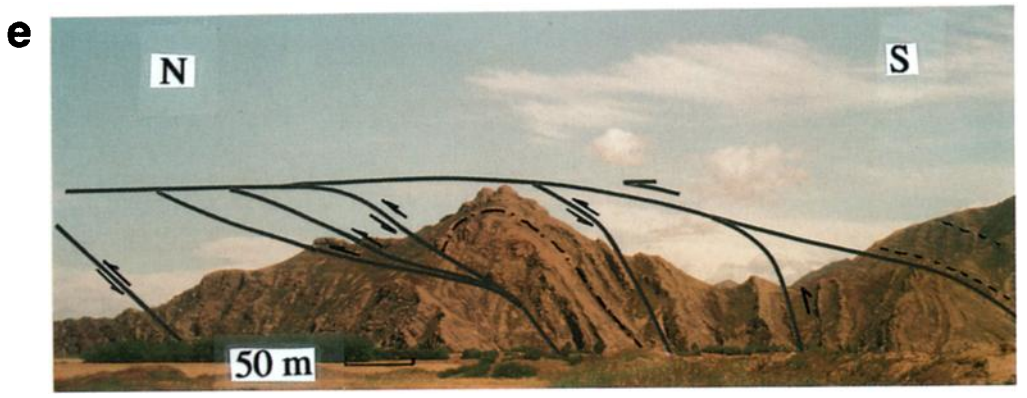

Plate 4. (continued)

developed in the Tethyan sedimentary rocks immediately above the fault in the Zedong area (Plate 5b), which also suggests a northward thrusting along the RZT. The RZT itself is crosscut by a N-S trending graben system, the Yadong-Gulu rift, that initiated at 8±1 Ma (T.M. Harrison et al., The Nyainqentanghla shear zone: Implications for Tibetan Plateau uplift and onset of the Asian monsoon, submitted to *Tectonics*, 1994].

Strike-Slip and Normal Faults

Both strike-slip and normal faults are observed locally near the "Indus-Tsangpo" suture in the Xigaze area. Near Renbu (Plate 1), an east-west striking, left-slip fault juxtaposes Cretaceous sedimentary rocks of the Xigaze Group to the south against Tertiary(?) conglomerates to the north, which unconformably rest on top of the Gangdese granites (Plates 6a and 6b). The structural significance of this fault is not clear. However, its structural position and faults with similar trend to the north mapped by Chinese geologists [*Liu et al.*, 1988] suggest that it may be part of a transfer fault system linking the NE-SW trending, late Miocene Nyainqentanghla normal fault system [*Pan and Kidd,* 1992] with a north-south trending normal fault system southwest of Xigaze.

West of Xigaze, right-slip faults trending between about N40°W and N10°E are also observed (Plate 2a). These faults displaced the GT between several hundreds to a few kilometers. Locally, these right-slip faults bend and strike parallel to the trace of the GT to form a series of small pull-apart basins (Plate 2a). The age relationship between the right-slip and left-slip faults is not clear. However, both sets of faults postdate the GT and their initiation and development may signal a marked change in the style of deformation.

Thermochronometry

Timing of Movement on the Gangdese Thrust

Mineral separates of K-feldspar, hornblende, biotite, and apatite were obtained from fresh hand specimens. For the $^{40}Ar/^{39}Ar$ analyses, mineral separates were irradiated together with Fish Canyon sanidine flux monitors for 45 hours in the H-5 position of the Ford Reactor, University of Michigan. Correction factors used for interfering neutron reactions were $(^{40}Ar/^{39}Ar)_K$ = 0.0225, $(^{38}Ar/^{39}Ar)_{Cl}$ = 1.20 x 10^{-2}, $(^{37}Ar/^{39}Ar)_{Ca}$= 7.00 x 10^{-4}, and $(^{36}Ar/^{39}Ar)_{Ca}$ = 2.90 x 10^{-4}. All samples were step heated in a Ta crucible within a double-vacuum furnace and $^{40}Ar/^{39}Ar$ isotopic measurements performed using a VG 1200S automated mass spectrometer operated in the electron multiplier mode. Details of flux monitor ages, neutron irradiation, step heating, and isotopic analyses are given by *Harrison et al.* [1992*b*]. Tabulated results of the argon isotopic analyses, uncorrected for neutron-produced interferences except $(^{38}Ar/^{39}Ar)_{Cl}$, are given in Table 1 using conventional decay constants and isotope abundances. The ZH-3 apatite separate was irradiated in the HIFAR reactor, Lucas Heights, Australia, and analyzed by the fission track method using techniques described by *Green* [1986]. Results are given in Table 2.

Zedong

$^{40}Ar/^{39}Ar$ and fission track thermochronometry were undertaken on two rock samples in the hanging wall of the GT near Zedong (Plate 3) with the intent of constraining the timing of thrusting. Sample locations are shown on Figure 1. ZH-3 is from an undeformed hanging wall granodiorite taken approximately 10 m above the top of the mylonitic shear zone. ZH-2b is a mylonitic granodiorite from within the >200-m-thick ductile shear zone.

The ZH-3 hornblende yields an $^{40}Ar/^{39}Ar$ age spectrum that drops from initial ages of ~50 Ma to ages over the last 80% of gas release of 31.6±1.5 Ma (Table 1). This latter age is substantially younger than all other dated plutons from the Gangdese batholith [e.g., *Copeland et al.*, 1987; *Honegger et al.*, 1982] and most certainly postdates the onset of collision. Clearly, this spectrum is disturbed and may have experienced both $^{40}Ar^*$ loss and uptake of excess $^{40}Ar^*$ making age interpretation difficult. We tentatively interpret the 32-Ma age to reflect the time of passage through the closure isotherm. Biotite from this sample yields an integrated total fusion age of 30.1±0.5 Ma (Table 1).

The coexisting K-feldspar yields a spectrum that is characterized by ages between about 24 and 29 Ma. Isothermal duplicate steps taken over the first 5% of gas release show a strong correlation on a plot of ΔCl/K (the difference in Cl/K between the two isothermal steps calculated from $^{38}Ar_{Cl}/^{39}Ar_K$) versus $\Delta^{40}Ar^*/K$ (i.e., the difference in

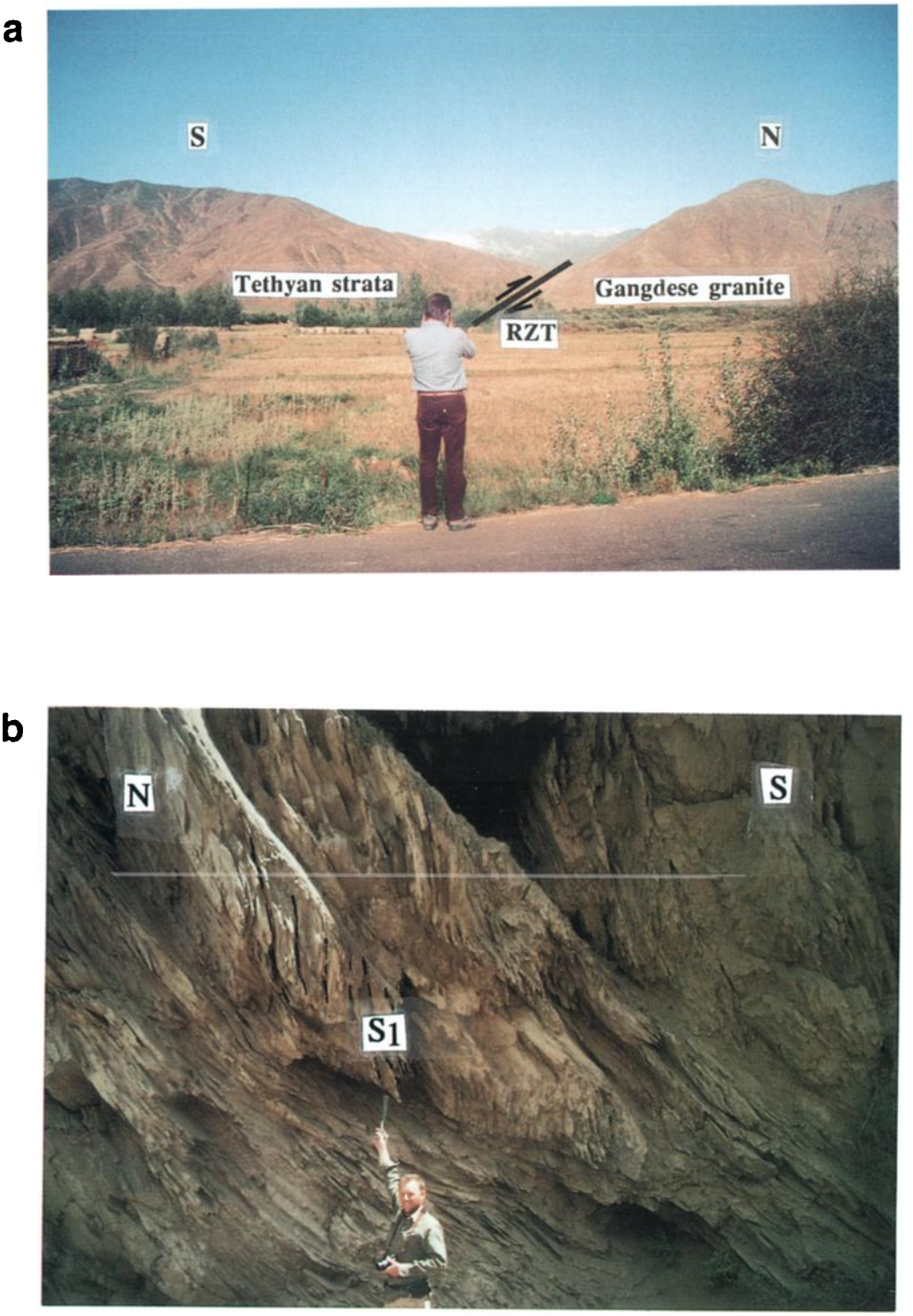

Plate 5. (a) The Renbu-Zedong thrust exposed near Gonggar. It juxtaposes the Tethyan strata over the Gangdese plutonic rocks. (b) South dipping cleavage (S_1) in Tethyan sedimentary rocks in the hanging wall of the Renbu-Zedong thrust near Zedong. In many places, the cleavage transpose the bedding completely, making the thickness estimate of the Tethyan strata difficult.

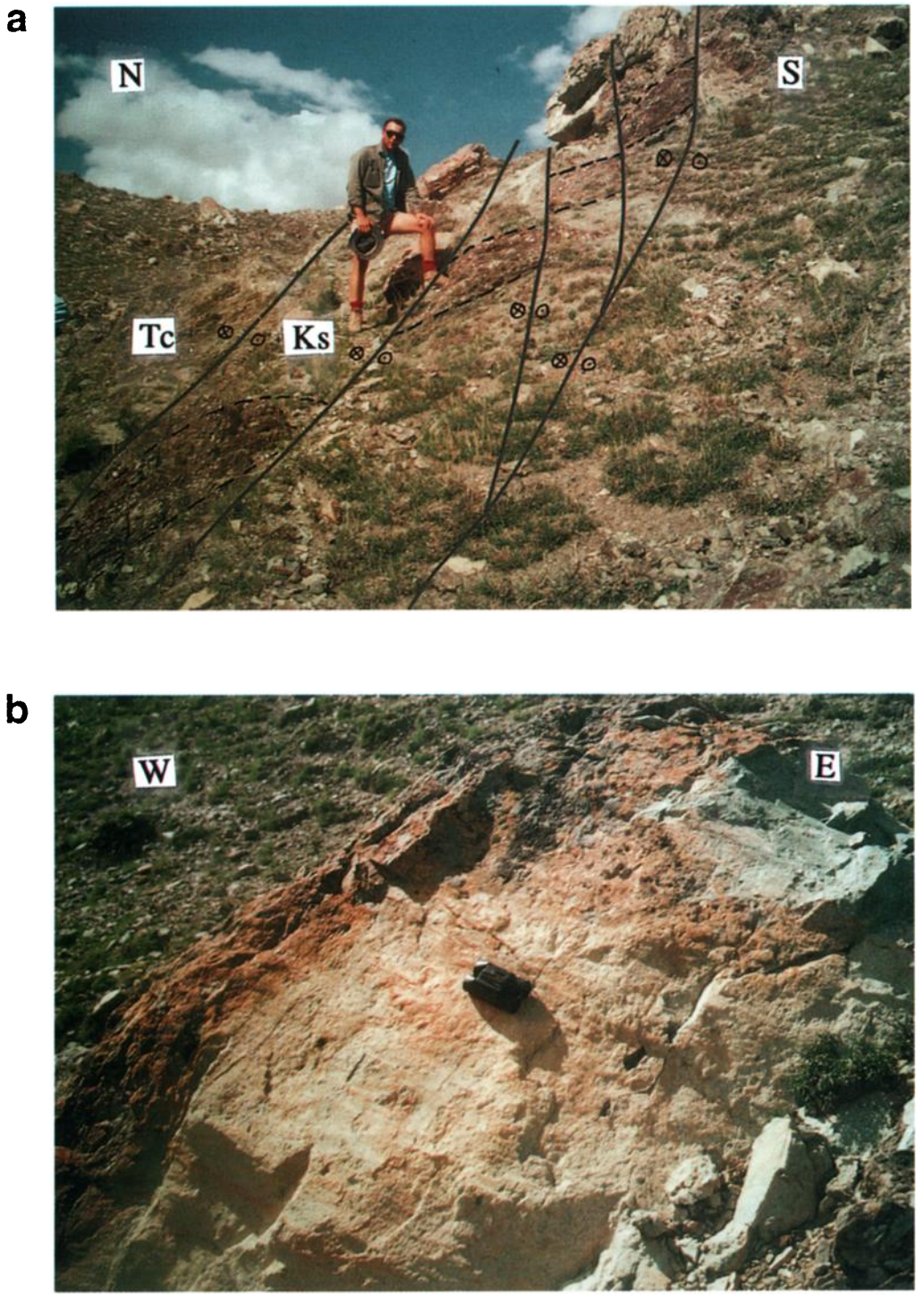

Plate 6. (a) E-W striking left-slip faults near Renbu. Note that the red-sandstone marker bed is offset laterally by several faults. (b) Subhorizontal striations on left-slip fault surfaces.

apparent age between the two steps) that indicate a Cl-correlated component of excess radiogenic argon of $^{40}Ar_E/Cl = 1.26\pm0.07 \times 10^{-5}$ [*Harrison et al.*, 1993b]. Recognition of this component allows identification of the fraction of excess $^{40}Ar^*$ present in each of the first 14 steps in the age spectrum (i.e., the product of the $^{40}Ar_E/Cl$ and Cl/K) and thus permits us to see through the contaminating effects of the Cl-correlated excess $^{40}Ar^*$ (Figure 2b). Although the age spectrum is highly irregular over the first 5% of gas release, ages corrected in this fashion yield a smooth age gradient from 25 to ~19 Ma.

Together with the associated Arrhenius parameters (Figures 2d and 2e), we have recovered the thermal history (Figure 2c) through the multidiffusion domain model [*Lovera et al.*, 1989,1991,1993; *Harrison et al.*, 1991,1992b; *Richter et al.*, 1991; *Fitz Gerald and Harrison*, 1993; *Leloup et al.*, 1993]. By correcting for Cl-correlated excess argon, we have obtained age information from 0.2 to 99% of ^{39}Ar released

Table 1. Argon Isotopic Results

Temperature °C	$^{40}Ar/^{39}Ar^{a}$	$^{38}Ar_{Cl}/^{39}Ar_{K}{}^{b}$	$^{37}Ar/^{39}Ar^{c}$	$^{36}Ar/^{39}Ar^{a}$ (10^{-3})	$^{39}Ar_{K}$ 10^{-15}mol	^{39}Ar Released %	$^{40}Ar^{*d}$,%	$^{40}Ar^{*}/^{39}Ar_{K}$	Age±1σ, Ma	Time, min	1000/T, K^{-1}	-log D/r^2, s^{-1}
ZH-2b K-Feldspar (J = 0.007822; Weight = 0.02100 g)												
400	65.26	0.0298	0.1986	219.6	0.438	0.023	0.45	0.3480	5±17	18	1.486	10.40
450	63.52	0.0241	0.1170	211.1	0.658	0.058	1.58	1.120	16±13	12	1.383	9.503
450	75.01	0.0190	0.1006	256.4	0.470	0.083	0	0	0	14	1.383	9.477
500	96.30	0.0169	0.0918	323.3	1.10	0.142	0.729	0.7356	10±14	10	1.294	8.761
500	33.22	0.0091	0.0667	107.5	3.14	0.310	4.09	1.423	2±3	27	1.294	8.434
550	8.527	0.0078	0.0593	21.9	3.18	0.479	20.1	2.030	28.4±1.5	10	1.215	7.756
550	2.894	0.0042	0.0504	4.01	4.34	0.710	41.8	1.691	23.7±0.5	15	1.215	7.619
500	3.123	0.0038	0.0453	2.66	0.516	0.738	45.8	2.317	32.4±1.0	20	1.294	8.583
600	3.340	0.0023	0.0699	4.69	11.8	1.37	51.5	1.937	27.1±0.3	20	1.145	7.060
600	1.549	0.0012	0.0786	0.0	5.02	1.64	73.7	1.877	26.3±0.3	17	1.145	7.207
500	4.394	0.0018	0.0487	0.01	0.612	1.67	41.4	1.840	25.8±2.5	50	1.294	8.549
650	2.981	0.0019	0.0778	3.31	7.79	2.08	54.9	1.988	27.8±0.3	10	1.083	6.690
650	1.928	0.0010	0.0718	0.018	11.0	2.67	80.1	1.906	26.7±0.1	13	1.083	6.549
700	2.948	0.0008	0.0647	3.31	33.9	4.48	63.1	1.955	27.4±0.1	11	1.028	5.813
700	1.960	0.0002	0.0571	0.082	25.4	5.83	88.9	1.918	26.9±0.1	14	1.028	5.883
750	2.332	0.0003	0.0530	1.35	52.5	8.63	78.9	1.916	26.8±0.1	10	0.9775	5.275
800	2.145	0.0002	0.0472	0.618	94.9	13.7	88.5	1.945	27.2±0.5	8	0.9320	4.733
800	2.024	0.0001	0.0452	0.197	81.2	18.0	95.0	1.947	27.3±0.1	13	0.9320	4.859
850	2.046	0.0	0.0476	0.258	173.	27.2	94.8	1.952	27.3±0.1	13	0.8905	4.375
850	2.011	0.0001	0.0438	0.097	59.1	30.4	96.0	1.964	27.5±0.1	12	0.8905	4.703
900	2.075	0.0001	0.0472	0.281	117.	36.6	95.1	1.973	27.6±0.1	9	0.8525	4.216
900	2.067	0.0	0.0422	0.260	133.	43.7	95.4	1.971	27.6±0.1	15	0.8525	4.302
950	2.132	0.0001	0.0405	0.443	148.	51.6	93.0	1.982	27.7±0.1	10	0.8177	4.005
950	2.150	0.0002	0.0335	0.458	180.	61.3	92.8	1.995	27.9±0.1	29	0.8177	4.286
1000	2.281	0.0005	0.0313	0.837	144.	69.0	88.3	2.014	28.2±0.1	28	0.7855	4.271
1050	2.432	0.0009	0.0328	1.30	74.5	72.9	83.3	2.027	28.4±0.1	13	0.7559	4.147
1050	2.527	0.0005	0.0329	1.55	42.1	75.2	81.1	2.050	28.7±0.1	15	0.7559	4.408
1100	2.682	0.0011	0.0432	2.09	77.3	79.3	76.2	2.045	28.6±0.1	20	0.7283	4.212
1100	2.789	0.0008	0.0460	2.34	59.0	82.4	74.5	2.079	29.1±0.1	30	0.7283	4.430
1100	2.956	0.0015	0.0499	2.80	43.8	84.8	71.4	2.112	29.6±0.2	42	0.7283	4.639
1100	3.181	0.0014	0.0543	3.32	50.6	87.5	68.6	2.182	30.5±0.2	91	0.7283	4.839
1100	3.830	0.0021	0.0623	5.23	83.2	91.9	59.2	2.269	31.7±0.2	413	0.7283	5.145
1100	5.886	0.0027	0.0713	11.7	24.1	93.2	41.2	2.423	33.9±0.3	305	0.7283	5.416
1100	6.024	–	0.0650	12.7	12.5	93.8	40.6	2.605	35.9±0.5	219	0.7283	5.499
1100	8.599	0.0030	0.0743	20.0	11.5	94.5	30.9	2.660	37.1±0.9	402	0.7283	5.751
1200	4.617	0.0046	0.1647	7.47	9.52	95.0	52.0	2.402	33.6±0.6	11	0.6789	4.228
1300	4.387	0.0039	0.0825	4.55	69.0	98.6	69.0	3.026	42.2±0.1	13	0.6357	3.166
1400	13.46	0.0050	0.1187	26.0	21.3	99.8	42.8	5.757	79.5±0.6	8	0.5977	2.813
1500	99.06	0.0232	0.5847	325.5	4.13	99.9	2.92	2.897	40±10	10	0.5640	–

Table 1. (continued)

Temperature °C	$^{40}Ar/^{39}Ar^{a}$	$^{38}Ar_{Cl}/^{39}Ar_{K}{}^{b}$	$^{37}Ar/^{39}Ar^{c}$	$^{36}Ar/^{39}Ar^{a}$ (10^{-3})	$^{39}Ar_{K}$ 10^{-15}mol	^{39}Ar Released %	$^{40}Ar^{*d}$,%	$^{40}Ar^{*}/^{39}Ar_{K}$	Age±1σ, Ma	Time, min	1000/T, K^{-1}	-log D/r^2, s^{-1}
ZH-3 K-Feldspar (J = 0.007184; Weight = 0.02467g)												
400	96.16	0.6663	0.1978	303.9	0.648	0.031	6.50	6.355	80.5±10.6	10	1.486	9.900
450	56.49	0.2960	0.1032	154.9	0.795	0.069	18.5	10.69	133±10.0	11	1.383	9.344
450	55.42	0.0689	0.1449	181.3	0.745	0.105	3.20	1.818	23.4±10.3	20	1.383	9.392
500	42.06	0.1322	0.0299	119.8	1.18	0.161	15.5	6.644	84.1±4.2	10	1.294	8.707
500	7.603	0.0125	0.0668	18.55	1.73	0.244	25.7	2.100	27.0±2.7	20	1.294	8.658
550	7.150	0.0481	0.0157	11.27	2.92	0.383	50.6	3.794	48.5±0.9	10	1.215	7.940
550	2.806	0.0046	0.0463	2.906	5.01	0.623	64.1	1.925	24.8±0.5	10	1.215	7.500
600	3.650	0.0138	0.0481	4.273	5.40	0.881	61.7	2.366	30.4±0.6	10	1.145	7.294
600	2.510	0.0022	0.0444	1.915	12.5	1.48	74.2	1.922	24.7±0.2	35	1.145	7.276
650	3.130	0.0078	0.0557	3.211	9.07	1.91	66.7	2.160	27.8±0.3	10	1.083	6.715
650	2.303	0.0005	0.0419	1.031	14.5	2.60	83.3	1.976	25.4±0.1	20	1.083	6.689
700	2.671	0.0036	0.0421	1.747	20.4	3.58	78.4	2.133	27.4±0.2	10	1.028	6.103
700	2.262	0.0002	0.0375	0.8380	31.6	5.09	86.8	1.992	25.6±0.1	28	1.028	6.212
750	2.377	0.0011	0.0687	1.152	21.5	6.11	83.2	2.017	26.0±0.1	10	0.978	5.821
750	2.232	0.0004	0.0401	0.6621	29.1	7.51	88.9	2.015	25.9±0.1	20	0.978	5.906
800	2.298	0.0007	0.0336	0.7547	29.6	8.92	88.0	2.053	26.4±0.1	10	0.932	5.517
800	2.210	0.0001	0.0339	0.5505	32.2	10.5	90.3	2.025	26.1±0.1	20	0.932	5.708
850	2.314	0.0004	0.0268	0.8072	29.4	11.9	87.4	2.052	26.4±0.1	10	0.890	5.386
850	2.238	0.0002	0.0271	0.6199	32.6	13.4	89.5	2.031	26.1±0.1	21	0.890	5.609
900	2.363	0.0007	0.0292	0.9624	26.4	14.7	85.6	2.056	26.4±0.1	10	0.853	5.332
900	2.237	0.0034	0.0249	0.7730	26.6	16.0	87.3	1.985	25.6±0.1	20	0.853	5.592
950	2.397	0.0007	0.0203	1.048	28.4	17.3	84.8	2.063	26.5±0.1	10	0.818	5.228
950	2.314	0.0007	0.0177	0.8431	32.1	18.8	87.0	2.041	26.3±0.1	21	0.818	5.460
1000	2.482	0.0013	0.0172	1.313	32.8	20.4	82.4	2.070	26.6±0.1	10	0.786	5.093
1000	2.437	0.0015	0.0171	1.135	56.8	23.1	84.6	2.077	26.7±0.1	28	0.786	5.257
1050	2.519	0.0021	0.0157	1.331	60.8	26.0	82.9	2.101	27.0±0.1	10	0.756	4.728
1050	2.412	0.0017	0.0163	0.9455	77.7	29.7	87.0	2.109	27.1±0.1	20	0.756	4.868
1100	2.384	0.0016	0.0134	0.8254	98.1	34.4	88.4	2.116	27.2±0.1	33	0.756	4.923
1100	2.411	0.0023	0.0144	0.8884	69.4	37.7	87.6	2.124	27.3±0.1	8	0.728	4.407
1100	2.352	0.0017	0.0123	0.7443	58.7	40.5	89.0	2.108	27.1±0.0	10	0.728	4.541
1100	2.357	0.0017	0.0142	0.6911	67.8	43.8	89.7	2.129	27.4±0.0	15	0.728	4.622
1100	2.350	0.0021	0.0178	0.6791	131	50.0	90.1	2.126	27.3±0.1	22	0.728	4.456
1100	2.364	0.0018	0.0176	0.6726	80.9	53.9	90.1	2.141	27.5±0.0	20	0.728	4.580
1100	2.393	0.0020	0.0191	0.6692	62.5	56.9	90.1	2.172	27.9±0.1	26	0.728	4.778
1100	2.416	0.0023	0.0231	0.7474	57.4	59.6	89.2	2.172	27.9±0.1	33	0.728	4.896
1100	2.451	0.0024	0.0256	0.7907	57.0	62.4	88.9	2.194	28.2±0.1	42	0.728	4.899
1100	2.467	0.0026	0.0258	0.8741	51.4	64.8	87.9	2.185	28.1±0.1	48	0.728	5.022
1100	2.491	0.0031	0.0271	1.009	55.9	67.5	86.5	2.170	27.9±0.1	66	0.728	5.091
1100	2.505	0.0029	0.0240	0.9584	54.4	70.1	87.1	2.198	28.3±0.1	87	0.728	5.188
1100	2.558	0.0031	0.0264	1.130	48.4	72.4	85.3	2.200	28.3±0.1	110	0.728	5.305
1100	2.609	0.0032	0.0268	1.250	57.3	75.1	84.4	2.216	28.5±0.1	183	0.728	5.413
1100	2.891	0.0033	0.0222	2.225	151	82.4	76.3	2.210	28.4±0.1	940	0.728	5.606
1100	3.056	0.0033	0.0224	2.928	32.1	83.9	70.2	2.167	27.9±0.1	351	0.728	5.755
1100	3.513	0.0036	0.0224	4.446	84.7	88.0	61.7	2.175	28.0±0.1	370	0.728	5.276

Table 1. (continued)

Temperature °C	$^{40}Ar/^{39}Ar^a$	$^{38}Ar_{Cl}/^{39}Ar_K{}^b$	$^{37}Ar/^{39}Ar^c$	$^{36}Ar/^{39}Ar^a$ (10^{-3})	$^{39}Ar_K$ 10^{-15}mol	^{39}Ar Released %	$^{40}Ar^*{}^d$,%	$^{40}Ar^*/^{39}Ar_K$	Age±1σ, Ma	Time, min	1000/T, K^{-1}	-log D/r^2, s^{-1}
ZH-3 K-Feldspar (J = 0.007184; Weight = 0.02467g) (continued)												
1100	4.074	0.0035	0.0195	6.415	46.6	90.2	52.6	2.155	27.7±0.2	394	0.728	5.455
1100	4.769	0.0034	0.0141	8.858	21.9	91.2	44.2	2.127	27.4±0.3	139	0.728	5.260
1200	2.469	0.0051	0.0101	0.6658	12.8	91.8	88.2	2.247	28.9±0.1	10	0.679	4.311
1300	2.403	0.0038	0.0100	0.4730	89.5	96.1	92.7	2.239	28.8±0.0	10	0.636	3.299
1400	2.898	0.0038	0.0184	1.856	65.3	99.2	79.8	2.326	29.9±0.1	10	0.598	2.958
1500	7.716	0.0051	0.1016	15.17	16.0	100	41.3	3.216	41.2±0.3	5	0.564	–
ZH-3 Biotite (J = 0.007852; Weight = 0.00594 g)												
600	132.3	0.2723	0.1410	446.4	3.46	0.776	0.264	0.3504	5±10	12		
700	3.224	0.0839	0.0724	8.24	8.70	2.73	22.4	0.7721	10.9±0.7	10		
780	3.233	0.0736	0.0205	4.72	17.8	6.71	54.3	1.817	25.6±0.2	8		
830	2.511	0.0712	0.0103	1.20	43.7	16.5	83.5	2.135	30.0±0.1	11		
880	2.272	0.0720	0.0878	0.403	65.6	31.2	92.6	2.131	29.9±0.1	20		
920	2.219	0.0725	0.0859	0.221	24.5	36.7	92.7	2.132	29.9±0.1	11		
920	2.229	0.0718	0.0820	0.222	18.7	40.9	91.7	2.142	30.1±0.1	18		
1020	2.412	0.0753	0.0297	0.616	44.8	50.9	90.0	2.210	31.0±0.1	11		
1100	2.467	0.0781	0.1440	0.841	78.5	68.5	88.6	2.208	31.0±0.1	8		
1150	2.447	0.0838	0.2780	1.05	35.2	76.4	85.3	2.137	30.0±0.1	5		
1200	2.424	0.0750	0.1159	1.08	59.3	89.7	85.2	2.094	29.4±0.1	5		
1450	8.246	0.0862	0.4645	20.8	46.0	100.0	24.3	2.109	29.6±0.3	7		
ZH-3 Hornblende (J = 0.007871; Weight = 0.01900 g)												
800	23.90	0.0842	0.5399	7.00	3.29	2.97	13.2	3.237	45.4±2.1	12		
900	12.94	0.0665	0.2904	3.18	3.91	6.49	26.5	3.563	49.9±1.4	10		
950	11.03	0.0674	0.5156	2.54	1.92	8.22	29.3	3.539	49.6±1.9	12		
1020	11.98	0.1421	2.928	3.22	2.09	10.1	20.7	2.689	37.8±2.2	8		
1035	11.80	0.2779	6.464	3.23	1.43	11.4	21.1	2.802	39.4±2.5	8		
1050	10.93	0.3736	8.389	2.89	2.16	13.3	26.0	3.095	43.4±1.9	10		
1070	9.549	0.4469	9.267	2.59	3.41	16.4	26.2	2.673	37.6±1.3	10		
1090	9.157	0.4903	9.459	2.49	5.55	21.4	27.0	2.591	36.4±1.5	11		
1110	8.422	0.5177	9.393	2.30	7.25	28.0	27.7	2.428	34.2±1.3	10		
1130	7.563	0.5284	9.444	2.09	5.15	32.6	27.4	2.192	30.9±1.1	16		
1150	8.007	0.5464	9.552	2.20	15.9	47.0	28.2	2.307	32.5±0.9	13		
1175	9.454	0.5475	9.670	2.74	11.1	57.0	22.5	2.177	30.7±1.0	8		
1200	14.029	0.5357	9.577	4.27	9.39	65.5	15.4	2.212	31.1±1.6	10		
1250	27.14	0.6024	11.08	8.71	6.02	70.9	8.46	2.342	32.9±2.7	8		
1300	23.12	0.6678	13.928	7.52	4.70	75.1	8.75	2.080	29.3±1.8	5		
1450	15.46	0.4118	7.772	4.72	27.6	100.0	14.0	2.187	30.8±1.4	5		

Table 1. (continued)

Temperature °C	$^{40}Ar/^{39}Ar^a$	$^{38}Ar_{Cl}/^{39}Ar_K{}^b$	$^{37}Ar/^{39}Ar^c$	$^{36}Ar/^{39}Ar^a$ (10^{-3})	$^{39}Ar_K$ 10^{-15}mol	^{39}Ar Released %	$^{40}Ar^*{}^d$,%	$^{40}Ar^*/^{39}Ar_K$	Age±1σ, Ma	Time, min	1000/T, K^{-1}	-log D/r^2, s^{-1}
					XH-9A K-Feldspar (J = 0.007158; Weight = 0.0200g)							
400	361.1	0.4135	0.4163	947.0	0.266	0.978	22.3	81.28	827±56	8	1.486	6.804
450	274.9	0.3089	0.3821	710.2	0.453	2.64	23.5	65.05	690±29	10	1.383	6.102
450	288.1	0.0650	0.4472	944.5	0.130	3.12	3.05	9.034	113±79	10	1.383	6.442
500	158.6	0.1795	0.4159	386.7	0.592	5.29	27.7	44.33	497±19	10	1.294	5.620
500	31.88	0.0284	0.4145	82.52	0.267	6.27	21.1	7.505	94±10	10	1.294	5.828
550	75.95	0.1097	0.8580	147.9	1.05	10.1	42.0	32.31	375±13	10	1.215	5.083
550	17.24	0.0135	1.981	29.18	0.484	11.9	45.3	8.763	109.8±4.1	10	1.215	5.290
600	46.77	0.0557	2.078	81.70	1.60	17.8	48.0	22.81	272.8±3.7	10	1.145	4.643
600	14.23	0.0043	1.847	17.37	0.708	20.4	59.0	9.231	115.4±2.2	10	1.145	4.887
650	31.02	0.0322	1.327	46.68	1.86	27.2	54.9	17.33	211.0±2.5	10	1.083	4.370
650	11.95	0.0015	0.7459	8.530	1.08	31.2	73.5	9.467	118.3±2.1	15	1.083	4.694
700	25.12	0.0251	0.3273	33.74	1.56	36.9	58.8	15.16	185.9±2.2	10	1.028	4.292
700	11.28	0.0013	0.1669	8.453	0.908	40.2	70.9	8.774	109.9±1.1	14	1.028	4.619
750	23.82	0.0213	0.2086	31.91	1.58	46.0	58.8	14.38	176.8±1.7	10	0.978	4.184
750	11.46	0.0001	0.1794	10.19	1.22	50.5	68.7	8.442	105.8±1.9	18	0.978	4.504
800	24.17	0.0204	0.3282	34.52	1.21	54.9	55.9	13.97	172.0±2.4	10	0.932	4.214
800	12.43	0.0026	0.2714	13.97	0.854	58.0	61.0	8.305	104.2±2.5	20	0.932	4.635
850	15.24	0.0013	0.4594	22.63	0.623	60.3	50.8	8.565	107.4±3.1	10	0.890	4.377
850	17.04	0.0023	0.4024	29.18	0.571	62.4	44.8	8.430	105.7±3.9	20	0.890	4.736
900	15.91	0.0059	0.4885	29.99	0.514	64.3	39.6	7.065	89.0±3.0	10	0.853	4.457
950	17.02	0.0081	0.6048	31.98	0.640	66.7	40.9	7.603	95.6±5.1	10	0.818	4.336
1000	21.88	0.0168	0.8255	45.50	0.539	68.6	35.7	8.486	106.4±4.7	10	0.786	4.383
1050	42.00	0.0558	1.165	90.85	0.656	71.0	35.0	15.24	187±8	20	0.756	4.568
1100	112.2	0.1706	1.543	212.2	0.892	74.3	43.8	49.66	549±12	33	0.728	4.608
1200	151.4	0.2225	1.663	261.4	3.94	88.8	49.0	74.31	770±12	10	0.679	3.251
1300	138.0	0.2227	1.645	246.1	1.21	93.2	47.1	65.48	694±7	10	0.636	3.467
1400	159.5	0.1752	1.366	354.9	0.514	95.1	33.9	54.80	597±31	10	0.598	3.655
1500	151.6	0.1281	0.9498	364.3	1.33	100	28.9	44.6	495±26	5	0.564	–
					XH-10B2 K-Feldspar (J = 0.007153 Weight = 0.0204g)							
400	154.2	0.0688	0.2275	508.3	1.58	0.404	2.55	3.952	50±18	10	1.486	7.670
450	52.56	0.0554	0.2051	164.0	3.06	1.18	7.73	4.089	52±5	10	1.383	6.788
450	25.62	0.0214	0.1827	83.18	1.49	1.56	3.91	1.027	13.2±3.8	10	1.383	6.863
500	15.16	0.0246	0.1425	43.68	5.62	3.00	14.6	2.237	28.6±1.1	10	1.294	6.066
500	3.346	0.0087	0.1172	7.247	4.72	4.21	33.5	1.191	15.3±0.5	14	1.294	6.089
550	3.406	0.0110	0.1300	5.253	12.6	7.42	52.8	1.841	23.6±0.2	10	1.215	5.310
550	1.954	0.0028	0.1848	2.481	9.35	9.81	58.8	1.213	15.6±0.2	12	1.215	5.347
600	2.856	0.0075	0.2870	4.107	9.86	12.3	55.5	1.643	21.1±0.3	10	1.145	5.136
600	2.047	0.0032	0.2914	2.219	10.4	15.0	64.9	1.392	17.9±0.2	10	1.145	5.023
650	4.318	0.0145	0.3579	6.703	27.4	22.0	53.8	2.344	30.0±0.1	10	1.083	4.470
650	2.202	0.0030	0.3908	2.579	13.0	25.3	63.6	1.449	18.6±0.2	10	1.083	4.686

Table 1. (continued)

Temperature °C	$^{40}Ar/^{39}Ar^a$	$^{38}Ar_{Cl}/^{39}Ar_K{}^b$	$^{37}Ar/^{39}Ar^c$	$^{36}Ar/^{39}Ar^a$ (10^{-3})	$^{39}Ar_K$ 10^{-15}mol	^{39}Ar Released %	$^{40}Ar^{*d}$,%	$^{40}Ar^*/^{39}Ar_K$	Age±1σ, Ma	Time, min	1000/T, K^{-1}	-log D/r^2, s^{-1}
XH-10B2 K-Feldspar (J = 0.007153 Weight = 0.0204g) (continued)												
700	2.419	0.0051	0.3632	2.997	34.5	34.1	62.9	1.540	19.8±0.1	17	1.028	4.394
700	1.731	0.0007	0.1665	1.514	7.78	7.78	68.5	1.274	16.4±0.1	10	1.028	4.737
750	2.142	0.0037	0.1996	2.318	25.5	42.6	66.5	1.450	18.6±0.1	24	0.978	4.553
750	1.948	0.0017	0.1363	2.589	3.85	43.6	53.1	1.717	15.1±0.3	10	0.978	4.953
800	3.042	0.0078	0.2732	4.298	12.7	46.8	56.7	1.771	22.7±0.2	10	0.932	4.416
800	2.095	0.0032	0.2071	2.473	7.02	48.6	60.7	1.358	17.4±0.2	10	0.932	4.649
850	3.397	0.0091	0.3117	5.284	10.2	51.2	52.6	1.838	23.6±0.3	10	0.890	4.467
850	2.210	0.0033	0.2771	2.935	4.83	52.5	55.5	1.342	17.2±0.2	10	0.890	4.775
900	2.681	0.0064	0.3448	4.451	8.85	54.7	49.0	1.371	17.6±0.3	10	0.853	4.498
900	2.340	0.0039	0.2511	3.573	5.39	56.1	50.7	1.282	16.5±0.3	12	0.853	4.778
950	2.814	0.0076	0.2622	5.013	8.82	58.4	45.4	1.330	17.1±0.4	10	0.818	4.471
950	2.971	0.0077	0.2049	5.660	5.91	59.9	41.1	1.292	16.6±0.4	12	0.818	4.710
1000	3.054	0.0097	0.1846	5.718	11.5	62.8	43.2	1.356	17.4±0.2	10	0.786	4.241
1000	3.316	0.0101	0.1699	6.442	8.80	65.1	40.9	1.403	18.0±0.4	12	0.786	4.454
1050	3.364	0.0147	0.1834	5.815	15.5	69.0	47.8	1.637	21.0±0.5	10	0.756	4.089
1050	3.840	0.0170	0.1810	6.972	13.3	72.4	45.2	1.771	22.7±0.3	16	0.756	4.308
1100	4.878	0.0279	0.2154	8.567	17.0	76.8	47.4	2.341	30.0±0.4	10	0.728	3.936
1100	6.270	0.0359	0.2197	10.96	28.1	84.0	48.0	3.028	38.7±0.3	37	0.728	4.169
1100	8.892	0.0491	0.2642	16.24	21.8	89.5	45.8	4.092	52.0±0.5	69	0.728	4.378
1100	12.64	0.0685	0.3374	23.98	12.8	92.8	43.7	5.562	70.4±0.5	77	0.728	4.482
1100	16.85	0.0865	0.4228	33.69	6.85	94.6	40.6	6.909	87.0±0.9	75	0.728	4.599
1100	33.82	0.1707	0.7698	68.48	18.7	99.3	40.2	13.63	168±2.0	928	0.728	4.818
1200	114.1	0.6420	2.586	209.2	0.719	99.5	45.4	52.58	576±10	10	0.679	3.669
1350	102.7	0.5319	3.555	193.8	1.12	99.8	44.1	45.83	512±14	10	0.616	3.231
1500	85.06	0.1983	1.166	220.7	0.809	100	23.1	19.93	241±16	5	0.564	–
XK-11 K-Feldspar (J = 0.007150 Weight = 0.02117g)												
400	183.9	0.3049	0.3279	591.7	0.864	0.481	4.87	9.013	114±18	10	1.486	7.518
450	112.0	0.3260	0.2843	338.1	1.01	1.04	10.7	12.07	149±18	10	1.383	6.948
450	65.90	0.0978	0.2344	210.9	0.669	1.42	5.29	3.567	45±7	14	1.383	7.066
500	81.75	0.2870	0.2152	237.4	1.40	2.20	14.1	11.61	144±9.0	10	1.294	6.432
500	32.63	0.0574	0.1987	101.8	0.997	2.75	7.58	2.550	33±6	10	1.294	6.444
550	24.21	0.1432	0.1906	59.85	2.67	4.24	26.5	6.514	82.1±1.8	10	1.215	5.866
550	8.714	0.0452	0.1795	22.04	1.59	5.12	23.5	2.194	28.1±1.5	10	1.215	5.965
600	26.05	0.1518	0.2457	62.35	5.62	8.25	29.1	7.621	95.7±1.5	10	1.145	5.261
600	15.50	0.0661	0.2789	38.73	7.62	12.5	26.0	4.058	51.6±1.3	23	1.145	5.300
650	49.17	0.2469	0.5427	127.5	4.45	15.0	23.3	11.51	143±4.5	10	1.083	5.050
650	18.30	0.0731	0.5710	48.29	7.14	18.9	22.0	4.053	51.5±1.2	10	1.083	4.754
700	15.82	0.0883	0.7829	39.50	15.4	27.5	26.4	4.190	53.3±1.0	10	1.028	4.282
700	4.163	0.0163	0.4959	8.670	2.87	29.1	35.9	1.619	20.8±0.8	10	1.028	4.926
750	4.084	0.0191	0.8760	7.703	16.7	38.4	44.7	1.855	23.8±0.3	11	0.978	4.126
750	2.312	0.0063	0.5068	3.439	6.41	42.0	53.2	1.313	16.9±0.3	10	0.978	4.425

Table 1. (continued)

Temperature °C	$^{40}Ar/^{39}Ar^a$	$^{38}Ar_{Cl}/^{39}Ar_K{}^b$	$^{37}Ar/^{39}Ar^c$	$^{36}Ar/^{39}Ar^a$ (10^{-3})	$^{39}Ar_K$ 10^{-15}mol	^{39}Ar Released %	$^{40}Ar^*{}^d$,%	$^{40}Ar^*/^{39}Ar_K$	Age±1σ, Ma	Time, min	1000/T, K^{-1}	-log D/r^2, s^{-1}
XK-11 Hornblende (J = 0.007150; Weight = 0.02117 g) (continued)												
800	5.258	0.0245	1.039	11.01	11.7	48.5	38.6	2.065	26.4±0.4	10	0.932	4.112
800	4.988	0.0241	0.7711	10.33	11.5	54.9	38.9	1.976	25.3±0.4	10	0.932	4.062
850	5.364	0.0240	0.6425	11.36	12.6	61.9	37.4	2.037	26.1±0.5	10	0.890	3.935
850	2.233	0.0044	0.4901	3.249	5.80	65.1	53.6	1.289	16.6±0.4	10	0.890	4.222
900	4.264	0.0138	0.4986	9.106	10.4	71.0	36.5	1.591	20.4±0.4	10	0.853	3.909
900	2.629	0.0057	0.3512	4.791	5.20	73.8	43.2	1.219	15.6±0.3	10	0.853	4.149
950	3.305	0.0083	0.3416	6.562	14.1	81.7	40.6	1.370	17.6±0.4	28	0.818	4.066
950	3.442	0.0081	0.3886	7.223	1.94	82.8	33.2	1.316	16.9±0.9	10	0.818	4.386
1000	3.544	0.0096	0.4852	6.695	3.53	84.7	41.3	1.582	20.3±0.5	10	0.786	4.087
1000	3.919	0.0108	0.5655	8.512	3.48	86.7	33.9	1.427	18.3±1.0	21	0.786	4.360
1050	5.319	0.0238	0.7200	11.70	3.50	88.6	33.8	1.896	24.3±1.0	10	0.756	3.971
1050	10.07	0.0619	1.217	24.22	3.32	90.4	28.8	2.987	38.1±1.7	24	0.756	4.302
1100	25.73	0.2249	2.523	61.00	2.85	92.0	30.2	7.903	99.2±2.7	12	0.728	3.990
1100	34.98	0.2799	2.070	84.65	1.66	93.0	28.4	10.12	126.0±4.9	28	0.728	4.526
1100	39.47	0.2753	2.448	99.52	1.36	93.7	25.5	10.26	127.7±4.9	65	0.728	4.928
1100	84.97	0.5746	3.838	218.6	2.88	95.3	24.2	20.73	249±4	961	0.728	5.684
1200	139.7	1.2721	4.522	328.3	0.527	95.6	30.4	43.16	485±20	11	0.679	4.401
1350	96.93	0.7770	5.353	225.2	5.90	98.9	31.7	30.90	360±8	10	0.616	3.032
1500	89.60	0.6294	5.624	219.5	2.00	100	27.9	25.26	300±7	5	0.564	–
XK-11 Hornblende (J = 0.007150; Weight = 0.02117 g)												
800	26.44	0.0280	28.16	90.04	1.67	1.57	7.62	2.103	26.9±4.4	10		
900	8.960	0.0431	18.90	29.73	1.63	3.09	17.3	1.681	21.6±1.4	10		
970	4.912	0.1878	7.043	13.45	2.10	5.06	27.4	1.484	19.0±1.0	10		
1020	3.227	0.2937	5.229	7.190	3.86	8.68	43.0	1.503	19.3±0.7	10		
1060	1.923	0.3328	5.429	3.550	30.0	36.9	65.6	1.289	16.5±0.2	10		
1090	1.975	0.3027	5.800	3.529	45.5	79.5	68.7	1.378	17.7±0.2	17		
1120	2.969	0.2291	6.869	6.893	2.57	81.9	43.4	1.465	18.8±1.0	10		
1170	2.204	0.3195	8.310	4.863	8.64	90.0	60.7	1.415	18.2±0.6	10		
1250	2.371	0.3249	9.401	5.681	9.94	99.4	57.4	1.429	18.3±0.4	10		
1450	44.78	0.3226	9.061	135.9	0.666	100.0	11.5	5.348	68±12	5		

[a] Corrected for background, blank, and discrimination.
[b] Corrected for background, blank, discrimination, atmospheric and K-derived argon.
[c] Corrected for background, blank, discrimination and decay of ^{37}Ar.
[d] Includes line blank.

Table 2. ZH-3 Apatite Fission Track Dating Results Calculated Using a Zeta of 353 for NBS Glass SRM 612

Parameter	Value
Number of grains	12
ρ_s, x 10^6 cm^{-2}	0.351
N_s	199
ρ_i, x 10^6 cm^{-2}	0.565
N_i	3207
(ρ_s/ρ_i)	0.062±0.005
$P(\chi^2)$	43.2
r	0.772
ρ_D x 10^6 cm^{-2}	1.447
N_D	154
Age, Ma ± 1σ	16±1
Mean track length, mm	12.78±0.39
Number of confined tracks	49
S.D., μm	2.77

The parameters are ρ_s, spontaneous track density; N_s, number of spontaneous tracks counted; ρ_i, induced track density; N_i, number of induced tracks counted; ρ_s/ρ_i, mean of individual crystal ratios (±1σ) for those analyses giving $P(\chi^2) < 5\%$; $P(\chi^2)$, probability of obtaining observed χ^2 value for v degrees of freedom (v is the number of crystals minus one); r, correlation coefficient between individual crystal track counts (N_s and N_i); ρ_D, track density measured in external detector adjacent to the glass dosimeter during irradiation; N_D, number of tracks counted in determining ρ_D; mean confined track length (±1σ); S.D., standard deviation of the track length distribution.

which corresponds to a temperature range of 160° to ~350°C. Uncertainty of the K-feldspar derived thermal history is estimated to be ±25°C and ±0.2 Ma [*Richter et al.*, 1991]. A second split of ZH-3 was run ($^{40}Ar_E/Cl$ = 1.44±0.25 x 10^{-5}) but detailed information is obscured by the fact that the sample was fused after only 63% of the gas had been released. Nonetheless, it yields a precise age over the initial gas release of 26.28±0.06 (1*s*) confirming that rapid cooling occurred at that time. Also shown on Figure 2 are the coexisting hornblende and biotite $^{40}Ar/^{39}Ar$ ages plotted assuming closure temperatures (T_C) of ~550°C [*McDougall and Harrison*, 1988] and 370±50°C (diffusion length scale, r = 0.34 mm [*Copeland et al.*, 1987]; activation energy, E = 47.0 kcal/mol, frequency factor, D_o = 0.077 cm^2/s [*Harrison et al.*, 1985]; and cooling rate, dT/dt = 100°C/m.y.), respectively.

Fission track analysis of the ZH-3 apatite yields an age of 16±1 Ma with a mean track length of 12.8±0.4 μm (Table 2). Together, these results correspond to an age of 18 Ma for the transit of this sample through the 110±10°C isotherm (Figure 2).

The age spectrum for ZH-2b K-feldspar is also suggestive of rapid cooling through the closure temperature interval at 27 Ma (Figure 3). The old ages in the late stages of gas release are likely not geochronologically meaningful but rather reflect excess argon. We have arbitrarily chosen not to use results beyond 90% ^{39}Ar release in the thermal calculations. No Cl-correlated excess argon component was detected in this sample. The log (r/r_o) plot of ZH-2b differs from ZH-3 in being convex upward rather than concave indicating a continuous (rather than discrete) distribution of subgrain sizes, possibly reflecting deformation-related recrystallization. The cooling histories of both rocks directly above the GT are shown together in Figure 3.

Age of Backthrusting

A lower limit on the age of the backthrust northwest of Xigaze (Plate 2) is constrained by dating of a north-south trending andesitic dike (sample XH-10B2) that cuts both the backthrust and its hanging wall structures. K-feldspar from this rock yields a complex spectrum with ages of ~18 Ma over the first 60% of gas release spectrum that then rise to >500 Ma (Table 1), undoubtedly due to excess argon. Oscillations in age in the early release again correlate with release of ^{38}Cl and yield an $^{40}Ar_E/Cl$ = 2.5±0.5 x 10^{-5}. Following correction for Cl-correlated excess argon for steps up to 900°C (beyond which point no argon release from fluid inclusions is indicated, an age of 15.4±1.5 (1σ) Ma is calculated between 15 and 65% ^{39}Ar released.

About 1 km east of this dike, a granitic sill can be traced within the Xigaze Formation for several kilometers. K-feldspar from this sill (sample XH-11), corrected for Cl-correlated excess argon using $^{40}Ar_E/Cl$ = 1.27±0.04 x 10^{-5}, yields an age of 14.0±1.0 Ma between 15 and 90% of ^{39}Ar release (Table 1) which is statistically indistinguishable from XH-10B2 K-feldspar. The coexisting XH-11 hornblende yields an age over the last 60% of gas release of 18.3±0.5 Ma, indicating that the K-feldspar ages are cooling dates. Since no andesitic magmatism of this age has previously been reported in southeastern Tibet, it is reasonable to assume that these two intrusives are coeval and date a phase of extensional magmatism that occurred at 18.3±0.5 Ma. We conclude that backthrusting had terminated in this region by that time. This is consistent with our hypothesis that the pop-up structure is a manifestation of the Gangdese thrust, and that thrusting ended during the early Miocene. The magmatism may reflect incipient collapse following late Oligocene-early Miocene crustal thickening via the GT.

A cobble from the conglomerate in the footwall of this thrust was dated in the hope of improving the Eocene (?) age constraint on the Qiuwu molasse [*Wang et al.*, 1983] and thus narrowing the possible duration of movement on the backthrust. K-feldspar from a granitic cobble (sample XH-9A) yields an age, once corrected for Cl-correlated excess argon ($^{40}Ar_E/Cl$ = 7.9±0.1 x 10^{-5}), of ~90 Ma. However this age, which corresponds to the oldest known plutonism in the Gangdese batholith [*Schärer et al.*, 1984], does not further constrain the age of the Qiuwu.

Discussion

Crustal Thickening in Southern Tibet

In our earlier tectonic model [*Harrison et al.*, 1992a], we proposed two scenarios for the rapid cooling of the eastern Gangdese batholith in the early Miocene recorded by thermochronometry: (1) movement on a north dipping normal fault along the northern margin of the Gangdese batholith caused rapid tectonic denudation; (2) movement on a north dipping thrust along the southern margin of the Gangdese batholith brought the Gangdese belt upward and southward onto the Indian continent (the hanging wall was rapidly eroded during or immediately after the thrust emplacement). Our field observations, together with earlier Chinese mapping, suggest that no significant normal faults are present along the northern margin of the plutonic belt, ruling out hypothesis 1. Instead on the northern margin we have observed south dipping thrusts in three separate locations that are possibly backthrusts of the GT. Recognition of the GTS relegates other mechanisms (climate change, tectonic denudation by normal faulting) [e.g.,

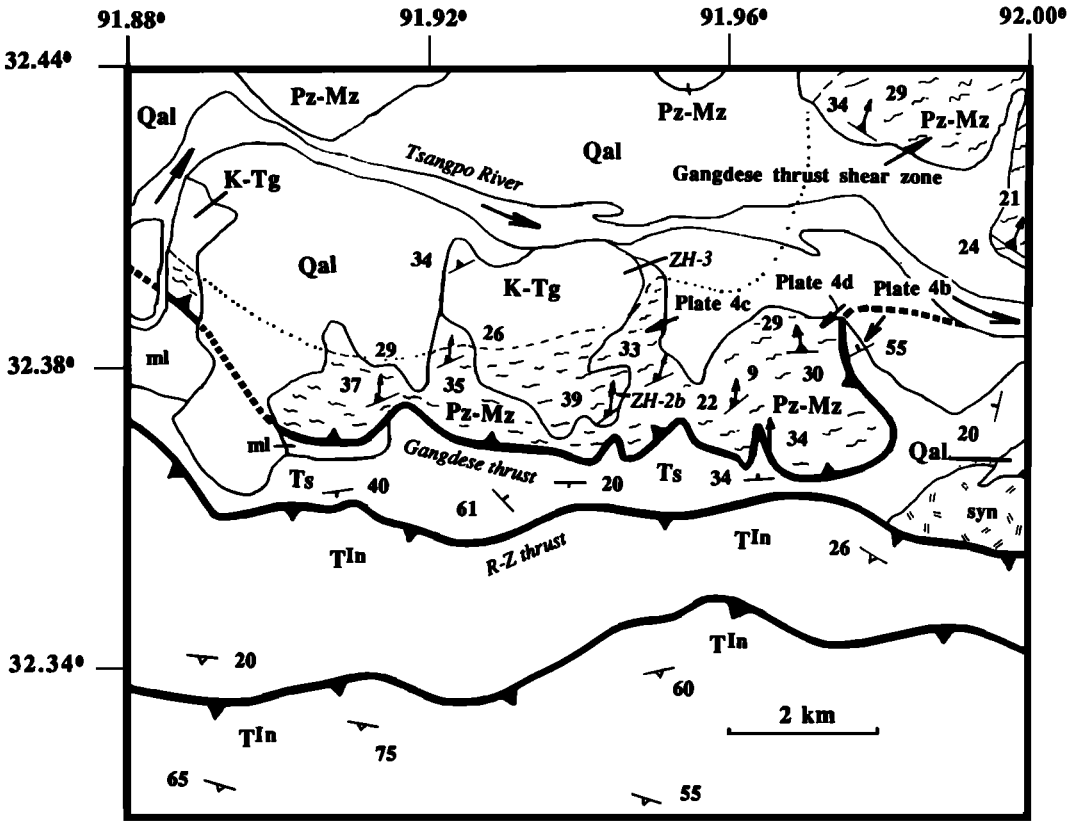

Figure 1. Simplified geologic map (see Plate 3a for map location) showing the locations of samples ZH-3 and ZH-2b relative to the trace of the Gangdese thrust. Also shown are the positions and angles from which Plates 4b, 4c, and 4d were taken. Rock units: Pz-Mz, metasedimentary rocks of the Lhasa block in the hanging wall of the Gangdese thrust; K-T_g, Cretaceous to Tertiary granite (= Gangdese batholith); ml, melange complex including highly sheared ultramafic rocks and isoclinally folded cherty shale and fine-grained cherty arenite; T_s, Tertiary conglomerate containing clasts of both the Gangdese granite and Tethyan sedimentary strata; syn, syenite of unknown age and origin in the footwall of the Gangdese thrust; T^{In}, Triassic strata of Tethyan sedimentary sequence, they bedding is mostly transposed by axial cleavage due to isoclinal folding; Q_{al}, Quaternary alluvium deposits. Foliation symbols: solid triangles indicate gneissic or mylonitic foliations, and open symbols indicate axial cleavage such those in the hanging wall of the Renbu-Zedong thrust. R-Z thrust, Renbu-Zedong thrust.

England and Molnar, 1990] to a supporting role in explaining the mid-Tertiary transition in cooling rate.

We have in earlier papers emphasized the role of erosional denudation in cooling midcrustal rocks following lithospheric thickening [*Copeland et al.*, 1987; *Richter et al.*, 1991; *Harrison et al.*, 1992a]. An additional cooling process implicit in the GTS hypothesis is refrigeration of the hanging wall as a consequence of thrusting [e.g., *Shi and Wang*, 1987]. The interplay between these two boundary conditions (i.e., denudation at the upper boundary, lateral heat flow at the base) produces three mid-Tertiary thermal regimes within the Gangdese thrust plate.

Regime 1. A zone exists directly above the thrust surface whose thickness is a function of the thermal time constant for the inferred duration of thrusting (maximum duration ~5 m.y.). In this zone, the thermal evolution is dominated by heat loss to the footwall. Because arrival of the footwall ramp is diachronous across the Gangdese batholith in the direction of thrust transport, this conductive length scale (i.e., the zone refrigerated by the footwall) might vary from ~10 km above the thrust surface in the south to only a few kilometers in the north.

Regime 2. Sufficiently far above the thrust surface, cooling is dominated by erosional denudation in response to thrust-related crustal thickening. Again, because thickening is diachronous, midcrustal rocks in the south will tend to be uplifted and denuded before rocks in the north.

Regime 3. A transition region exists between regimes 1 and 2 in which cooling is due to both processes.

Near the thrust surface (regime 1) we see evidence for rapid cooling beginning at 27 Ma that we interpret to result from refrigeration by the cold Tethyan sediments. This event is observed not only at Zedong, but also 60 and 120 km further west along strike, respectively, at Samye and Quxu (Plate 1) [*Copeland et al.*, 1994]. This concordance of ages within regime 1 is perhaps the best evidence that thrusting was underway at 27 Ma. Note that the observed pattern of cooling in the Gangdese batholith is the opposite of what would occur if the RZT had been the dominant structural control.

The geological relationships characterizing the rocks east of Zedong are similar in at least two respects with those ~1100 km to the west. In the vicinity of Mount Kailas, the absence of the Xigaze strata is again correlated with an early Miocene uplift/unroofing pulse suggesting that the GTS may

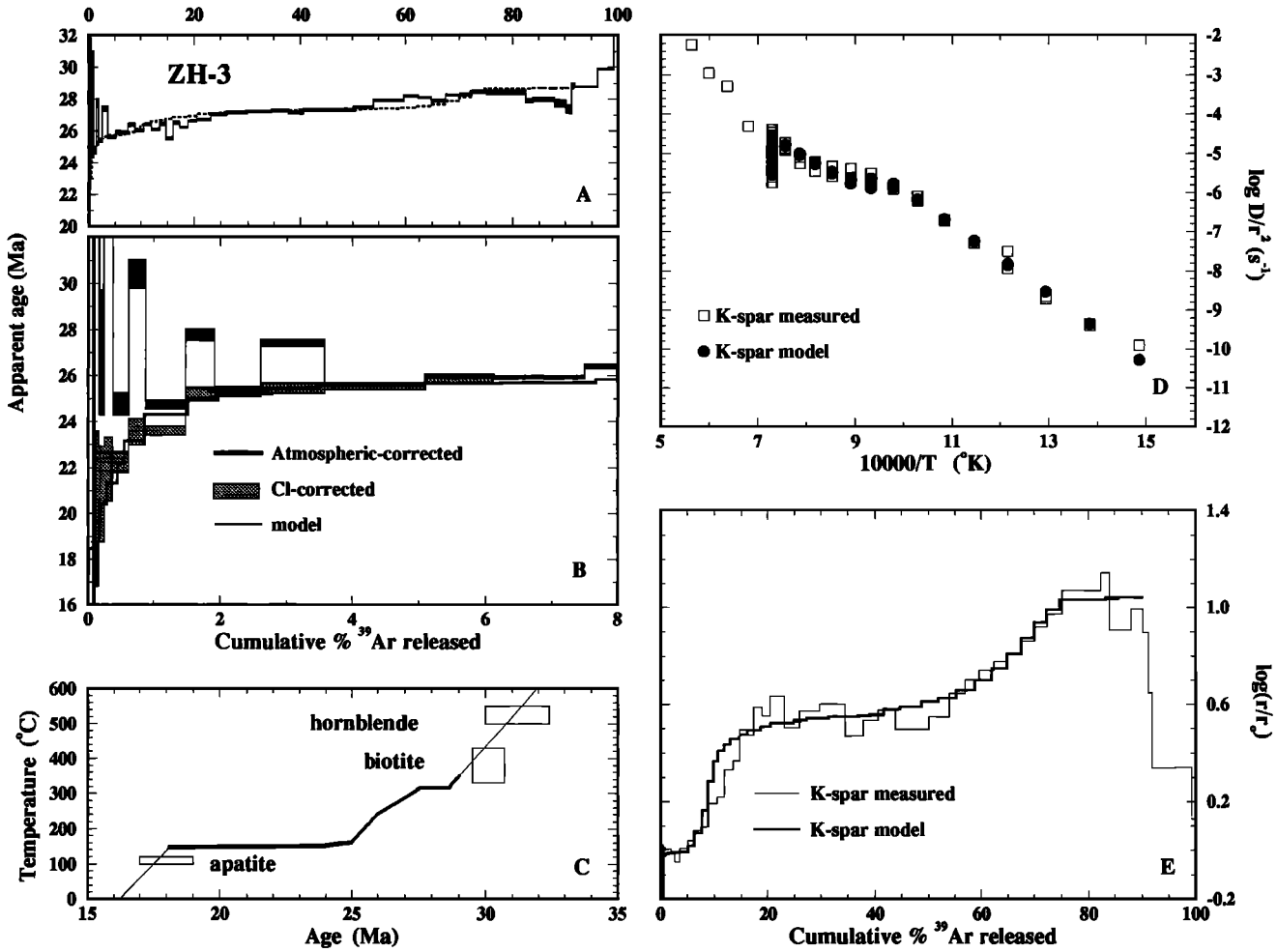

Figure 2. ZH-3 (a) $^{40}Ar/^{39}Ar$ spectrum and modeled fit; (b) an expanded view of the first 8% of gas release showing the change to the age spectrum from correction for Cl-correlated excess $^{40}Ar^*$; (c) the calculated thermal history (the portion constrained by the K-feldspar is shown by the thick line); (d) the Arrhenius plot calculated from ^{39}Ar diffusivities together with the model fit; and (*e*) the log (r/r_o) plot. Model fit parameters are, E = 41.7 kcal/mol; log (D_o/r^2) and volume fractions of the eight domains are (1) 7.86/0.0005, (2) 5.37/0.023, (3) 5.28/0.041, (4) 2.41/0.361, (5) 2.40/0.155, (6) 1.10/0.285, (7) 1.09/0.133, (8) -0.83/0.0015. Also shown in (*c*) are $^{40}Ar/^{39}Ar$ ages for biotite and hornblende and an apatite fission track result (see text for T_c information).

have been active over at least 1100 km along strike [*Liu et al.*, 1988; *Harrison et al.*, 1993a]. Variations in the magnitude of displacement along strike of the GT may be due to the transfer of displacement to thrusts in the Tethyan Himalaya (= Southern Tibetan Zone), irregularity of the northern boundary of the Indian continent, or different curvatures of the Gangdese arc and the northern Indian continental margin.

Minimum Slip and Slip Rate Along the Gangdese Thrust

The rate of slip along the GT can be calculated from its minimum displacement (46±9 km) divided by the duration of thrusting, estimated from thermochronometry to be 4±2 m.y. This latter figure is based on considerations of the time difference between the onset of thrust-related cooling near Zedong (at 27 Ma) and the time at which uplift-related denudation was initiated ~60 km to the north (at circa 23 Ma), described in the next section [*Copeland et al.*, 1987, 1994; *Richter et al.*, 1991]. This suggests a minimum slip rate of 12±6 mm/yr, which is similar to the present rate of convergence at the southern edge of the collision zone [*Molnar and Deng*, 1984; *Avouac and Tapponnier*, 1993].

Relationship of the GTS to Previous Thermochronometry

We have previously pointed to thermochronological results in the Gangdese batholith as evidence that this belt in southern Tibet experienced rapid denudation in response to crustal thickening during the late Oligocene-early Miocene [*Copeland et al.*, 1987, 1994; *Richter et al.*, 1991; *Harrison et al.*, 1992a, 1993a]. Our present observations appear to provide a mechanism that explains the pattern of cooling ages throughout the Gangdese batholith. Assuming a flat-ramp geometry for the GT, with the flat following the brittle-ductile transition at ~15 km depth, the tip of the footwall ramp would propagate northwards at the same rate as the GT, estimated to be at least 12 mm/yr. At this rate, the Gangdese batholith near Lhasa, originally resting on the thrust flat, would not be transported up the ramp of the GT (and thus

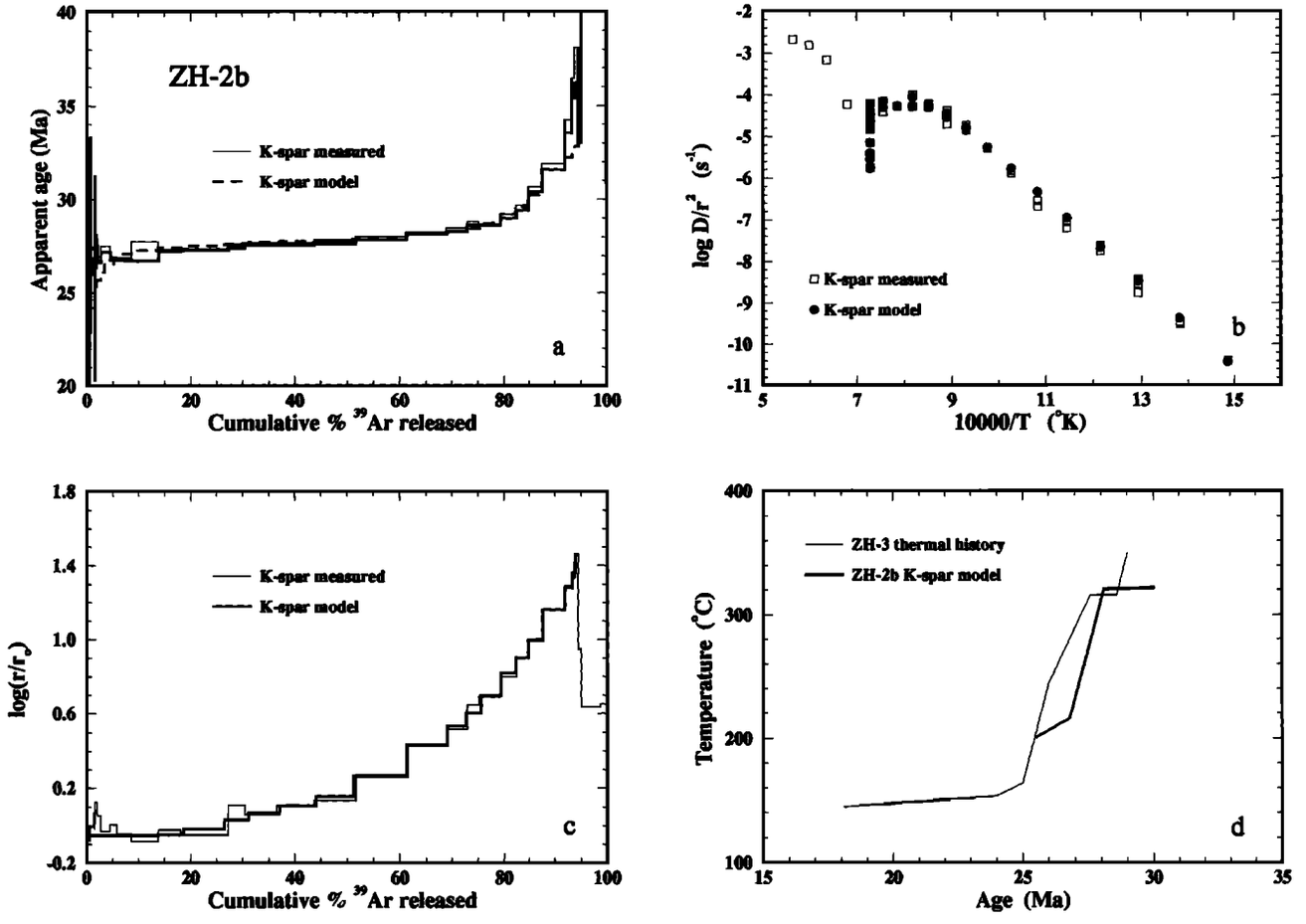

Figure 3. ZH-2b K-feldspar (*a*) $^{40}Ar/^{39}Ar$ spectrum and modelled fit; (*b*) the Arrhenius plot calculated from ^{39}Ar diffusivities together with the model fit, (*c*) log (r/r_O) plot, and (*d*) calculated thermal history (heavy line). Also shown is the thermal history derived for ZH-3. Model fit parameters are: E = 46.5 kcal/mol; log (D_o/r^2) and volume fractions of the nine domains are (1) 5.80/0.108, (2) 4.88/0.028, (3) 4.87/0.247, (4) 4.86/0.091, (5) 4.11/0.222, (6) 3.38/0.124, (7) 2.61/0.060, (8) 2.49/0.061, 0.57/0.059.

uplifted and subsequently denuded) until 23-22 Ma. The widespread preservation of precollisional Linzizong volcanic rocks along the northern margin of the Gangdese Shan [*Liu et al.*, 1988] and the relatively modest amount of post-22 Ma denudation (and thus thickening) in the vicinity of Lhasa (<4 km) [*Copeland et al.*, 1994] suggest that the northern tip of the footwall ramp did not extend beyond the northern margin of the Gangdese batholith. Thus we infer that movement on the GT terminated at 23-22 Ma. If our assumptions regarding the GT fault geometry are correct, a total displacement of 60 km would be implied.

Thermochronological results from two regime 2 locations in the Gangdese batholith, about 30 km north of Quxu (Plate 1), reveal clear evidence of rapid cooling beginning at about 20 Ma [*Copeland et al.*, 1987; *Richter et al.*, 1991]. These data were interpreted to reflect enhanced denudation due to isostacy-driven uplift. Because there is a ~2 m.y. lag between the onset of rapid denudation and significant

Plate 7. Cross-sectional views of the tectonic development of the southern Tibetan plateau and Higher Himalaya. (a) 100-60 Ma: North dipping subduction consuming the oceanic lithosphere between India and Asia. (b) 60-50 Ma: Volcanic eruptions that produced the Linzizhong volcanics. (c) 50-35 Ma: Subduction of the thinned northern margin of the Indian continent beneath the thin crust of the southern margin of the Lhasa Block that is made of mostly the accretionary wedge. (d) 35-27 Ma: Further convergence between India and Asia along the suture zone that produced thickened crust in the southern margin of the Lhasa Block. At about 27 Ma, the Gangdese thrust began to develop. (e)-(h) 27-20 Ma: Structural events occurred during this period are (from older to younger), (1) movement along the Gangdese thrust that brought the Gangdese plutonic rocks over the Tethyan sediments and the development of the backthrust that puts the Xigaze strata over the Gangdese plutonic rocks and Tertiary conglomerates, and (2) the development of the Renbu-Zedong thrust as a back thrust of the Main Central Thrust and the thrust toe of the High Himalayan normal fault system.

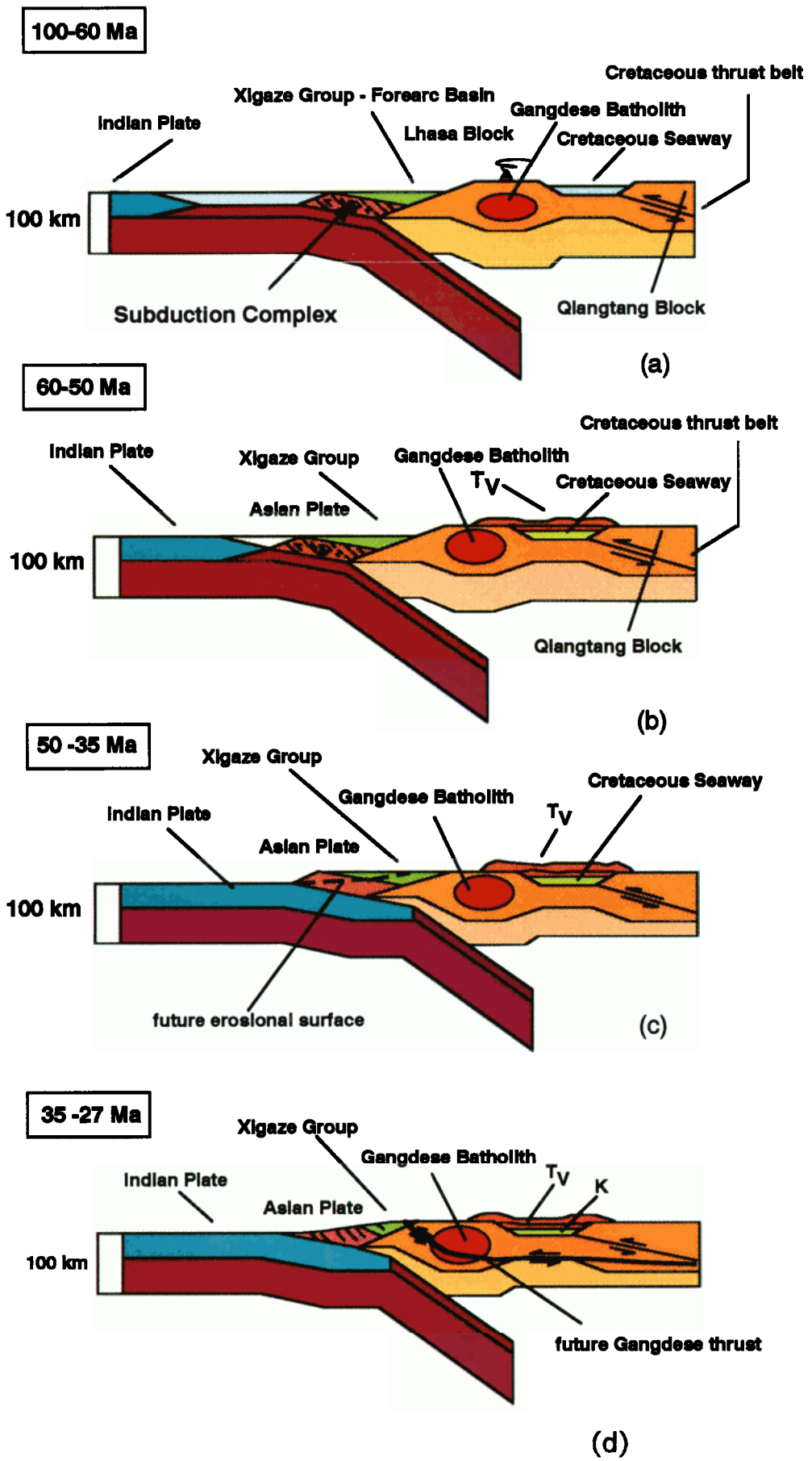
100-60 Ma
Cretaceous thrust belt
Xigaze Group - Forearc Basin
Gangdese Batholith
Indian Plate
Lhasa Block
Cretaceous Seaway
100 km
Subduction Complex
Qiangtang Block
(a)
60-50 Ma
Cretaceous thrust belt
Indian Plate
Xigaze Group
Gangdese Batholith
Tv
Cretaceous Seaway
Asian Plate
100 km
Qiangtang Block
(b)
50 -35 Ma
Xigaze Group
Cretaceous Seaway
Gangdese Batholith
Indian Plate
Tv
Asian Plate
100 km
future erosional surface
(c)
35 -27 Ma
Xigaze Group
Gangdese Batholith
Indian Plate
Tv
K
Asian Plate
100 km
future Gangdese thrust
(d)

initiation of cooling in the midcrust [*Copeland et al.*, 1987; *Richter et al.*, 1991], crustal thickening at these locations can be inferred to have occurred at 23-22 Ma. The coincidence between this age and the presumed time of arrival of the GT in the northern Gangdese batholith appears to implicate it as the thickening mechanism responsible for the observed pulse of late Oligocene-early Miocene uplift. Because virtually all active crustal scale thrusts around the Tibetan plateau surface at elevations < 2000 m, we may presume that the southeastern Tibet was at an elevation between 0 and 2000m during the development of the Gangdese thrust system.

Age Constraints on Movement of the Main Central Thrust

The Main Central thrust (MCT), generally believed to be the earliest of the crustal scale thrusts developed on the Indian continent, is thought to have experienced between 100 and 250 km of south directed displacement [e.g., *Gansser*, 1981; *Lyon-Caen and Molnar*, 1983, 1985; *Bouchez and Pêcher*, 1981]. Although cooling ages of minerals from the shear zone place an approximate lower age limit of ~17 Ma (see *Hubbard and Harrison* [1989] for a review), details of the timing of thrusting, particularly of initiation, remain poorly known. From thermobarometric and thermochronological considerations, *Hubbard and Harrison* [1989] argued that metamorphism of the MCT in response to tectonism was in progress at 20.9±0.3 Ma near Mt. Everest. *Parrish and Hodges* [1993] concluded that ductile deformation within the MCT near Annapurna terminated at 22±1 Ma. The oldest established age of anatectic material thought to be derived from MCT related activity is the 24-Ma Makalu leucogranite [*Schärer*, 1984]. *Copeland et al.* [1990,1991] concluded that anatexis due to thrusting was probably largely completed by 18 Ma, suggesting a similar age for termination of large-scale slip.

Our thermochronological results from the GT near Zedong may bear on the age of initiation of the MCT. As discussed above, we infer from geological and thermochronological considerations [*Copeland et al.*, 1987; *Richter et al.* 1991; *Harrison et al.*, 1992a] that the GT was active between 27 and ~23 Ma. It is generally believed that the initiation of major thrust motion in the Himalaya has moved sequentially toward the foreland during the collision [*Gansser*, 1981]. If so, this and other lines of evidence mentioned above constrain the timing of the most significant MCT activity to be between about 24 and 21 Ma.

Relationship Between the MCT, North Himalayan Fault, and Renbu-Zedong Thrust

It is possible that the MCT, the North Himalayan (normal) fault (NHF), and the RZT are related products of the same evolving mechanical system. In the Rongbuk valley, an early phase of the North Himalayan normal fault system [*Burg et al.*, 1984; *Pêcher*, 1991; *Burchfiel et al.*, 1992] is cut by an essentially undeformed granitoid that has been precisely dated at 21.7±0.5 Ma [cf. *Copeland et al.*, 1988; *Parrish*, 1990; T.M. Harrison et al., Identification of inherited monazite in the Manaslu leucogranite by $^{208}Pb/^{232}Th$ ion microprobe dating, submitted to *Nature*, 1994], placing a lower age limit on fault motion. Thus the earliest phase of movement appears to have been prior to 21.2 Ma, possibly coeval with our estimate made above for the movement on the MCT. Later movement within the NHF certainly postdates ~11 Ma [*Maluski et al.*, 1988] and may be relatively recent [*Burchfiel et al.*, 1992]. *Yin* [1993] proposed a mechanical link between the MCT and NHF; using an elastic approximation it could be shown that the state of stress is critically dependent on pore-fluid pressures both along and within the wedge-shaped hanging wall of the MCT. Within the model framework, the onset of partial melting [*LeFort*, 1986] above the thrust zone produced the parent of the magma that later crosscuts the NHF. Anatexis within the hanging wall would act as a tremendous sink for the volatiles evolved during metamorphism of the lower plate, thereby reducing the pore fluid pressure along the thrust and creating stress conditions in the hanging wall favorable for initiation of normal faulting. This could explain the virtual synchroneity of the MCT and the earliest phase of movement on the NHF. Once the NHF was initiated, continued motion at a low angle is likely if a high pore fluid pressure in the fault zone is present [e.g., *Axen*, 1992].

North-south extension in the Higher Himalaya between the early Miocene and Pliocene may have been partially or completely compensated by motion on the RZT. L. Ratschbacher et al. (Distributed deformation in southern and western Tibet during and after the India-Asia collision, submitted to *Tectonophysics*, 1993) obtained a 17.5±0.9 Ma K-Ar age from white mica filling a tension gash in the RZT shear zone near Renbu. Although possibly a cooling age, the low grade of metamorphism affecting these rocks likely did not exceed the white mica closure temperature of ~350-400°C. The circa 18 Ma age is consistent with the known timing of the NHF. Our proposed structural model suggests that the extension was restricted to the Higher Himalaya and synchronous with both contraction south (MCT) and north (RZT) of the normal fault system.

Role of Precollisional Thrusting in the Formation of the Tibetan Plateau

Whether the presently high elevation of the Tibetan plateau was caused by the Indo-Eurasia collision alone, or was contributed to by crustal thickening prior to the collision, is a controversial [*Kidd et al.*, 1988; *England and Houseman*, 1986; *England and Searle*, 1986] issue that is central to determining the crustal mass balance during collision [e.g., *Le Pichon et al.*, 1992; *England and Houseman*, 1986; *Richter et al.*, 1992]. Our preliminary mapping in the Chuoqin area, south-central Tibet (Figure 1), suggests that crust in this region was thickened by at least 40-50% over a belt 40-70 km wide by thrusting and folding. There, Paleozoic-Mesozoic strata were involved in southward thrusting and south verging folding. Thrusts were intruded by an Early Cretaceous granite (T. M. Harrison, unpublished data, 1993) and rest unconformably below Paleocene Linzizong volcanic strata. Similar structures are also observed north of Lhasa in the Mezhugongka area (Plate 1), where the folded Cretaceous Takena Formation is overlain unconformably by the Paleocene Linzizong volcanics. Deposition in southern Tibet of widespread Cretaceous clastics, containing medial Cretaceous marine beds, may have occurred in a foreland basin produced by loading of thrust sheets to the north after closure of ocean(s) between the Lhasa and Qiangtang blocks (Plates 7a and 7b). Somewhat thickened crust may have remained from this convergent event in the northern part of the Lhasa block at the time of initiation of the Indo-Asian collision.

Why Did the Gangdese Thrust Begin Movement 20 m.y. After the Initial Collision?

Although somewhat uncertain, it seems likely that the collision of India with southern Asia was underway by about 50 Ma [*Dewey et al.*, 1989; *Peltzer and Tapponnier*, 1988].

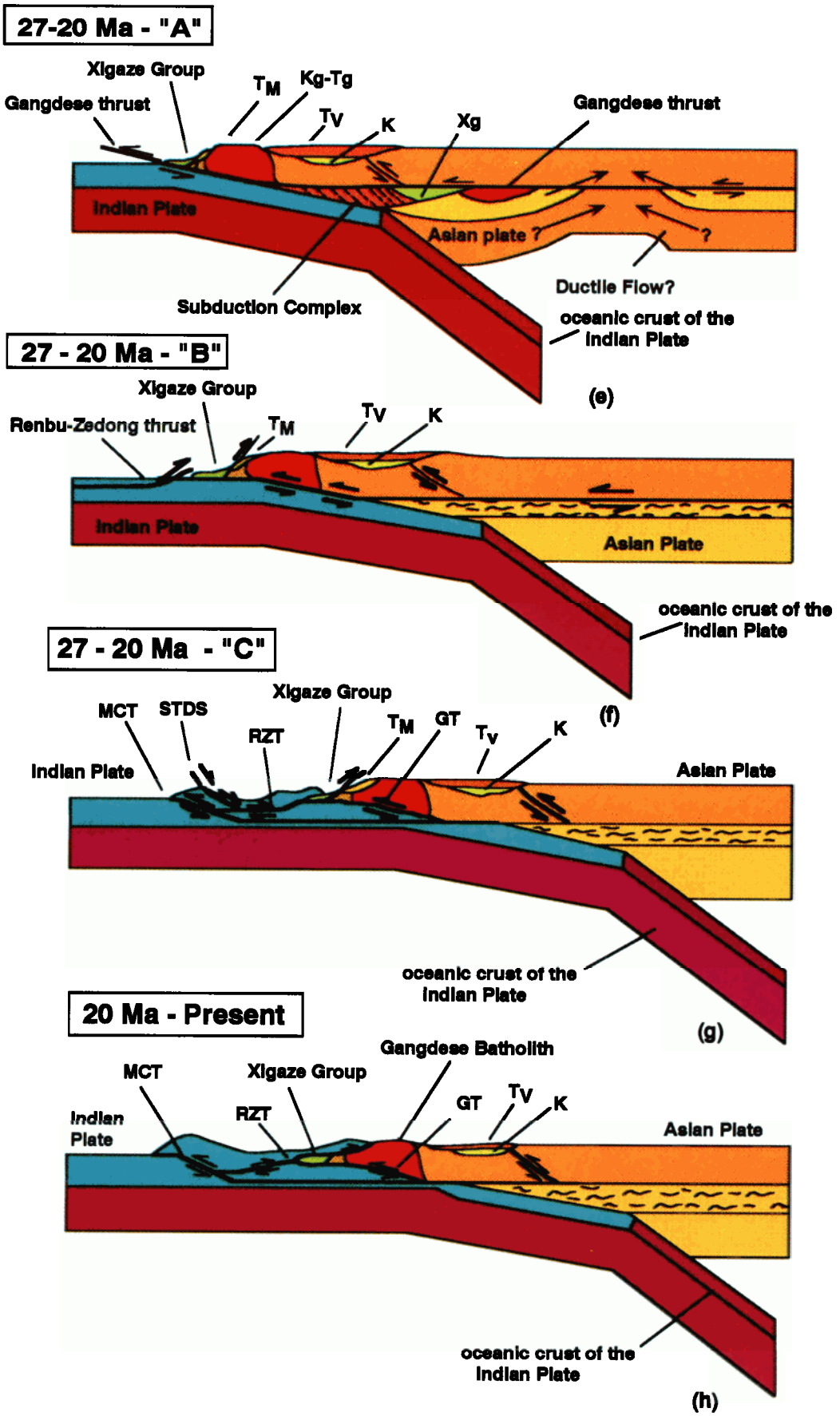

Plate 7. (continued)

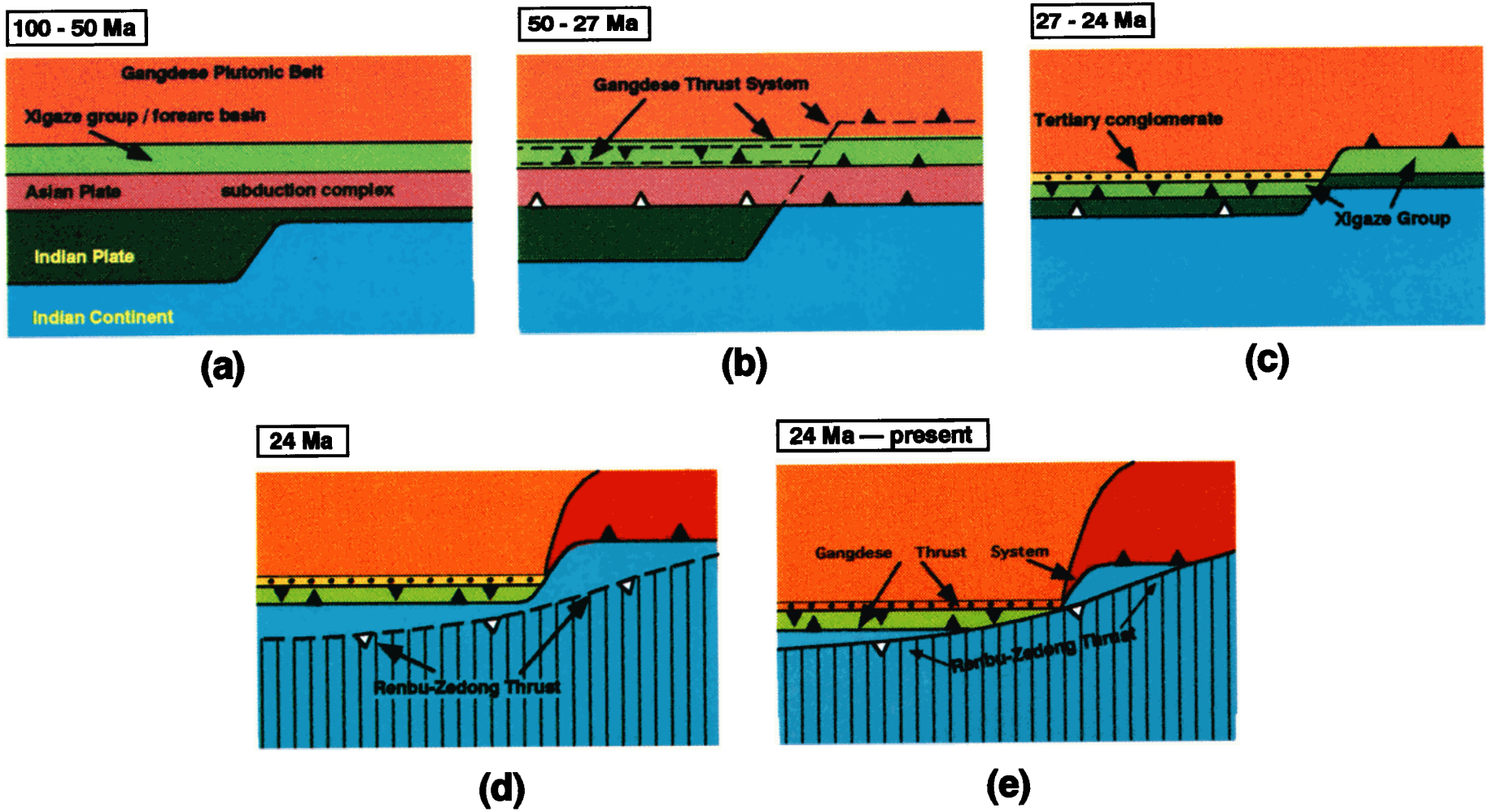

Plate 8. Tectonic development of the southern Tibetan plateau on map view. (a) 100-50 Ma: The northern edge of the Indian continent is an irregular geometry due to earlier rifting events. (b) 50-27 Ma: In response to the indentation of the irregular northern Indian margin, the GTS was developed with the deformational style changing along its strike, i.e., a single thrust (GT) was initiated east of Renbu, and a pop-up structure bounded by both the GT and a backthrust. (c) 27-24 Ma: The accretionary complex, Xigaze strata, and part of the Gangdese batholith began to be underthrust beneath the Gangdese thrust. (d) 24 Ma: The Xigaze Group and southern part of the Gangdese batholith were underthrust beneath the eastern segment of the Gangdese thrust. End of motion along the Gangdese and the initiation of the Renbu-Zedong thrust. (e) 24 Ma - present: The northward motion along the Renbu-Zedong thrust obscures the trace of the GT, and locally juxtaposes the Tethyan strata over the Gangdese granitic rocks.

However, the southernmost thrust system of the Lhasa Block, the GTS, apparently did not begin to move until about 27 Ma or ~23 m.y. after collision began. This observation appears to contradict the prediction of *England and Houseman* [1986] that deformation due to indentation of India should have started first along the southern margin of the Eurasian continent. Why then was significant deformation along the southern margin of Asia delayed for so long? It is possible that tectonic extrusion along major strike-slip faults, such as the Red River ductile shear zone [*Peltzer and Tapponnier*, 1988; *Tapponnier et al.*, 1982], and crustal shortening along major crustal-scale thrusts farther north of the suture [*Chang et al.*, 1986] permitted the deformation front to migrate southward from the Kunlun Shan region south of the Qiadam basin towards the southern margin of the Lhasa Block (rather than the reverse).

Tectonic Model

On the basis of the geologic relationships and thermochronological analyses discussed above, we propose a tectonic model for the evolution of the southeastern Tibetan plateau since the late Cretaceous, shown in both cross-sectional (Plate 7) and map views (Plate 8). Note that Figure 7 depicts only the tectonic history of the GTS east of Renbu.

Subduction of the Indian plate beneath the Eurasian continent between 100 and 50 Ma produced an Andean-margin system in southernmost Asia that includes the Gangdese batholith and Linzizong volcanics as the volcanic arc, the Xigaze strata as forearc deposits, and possibly an accretionary complex (Plate 7a). The northern edge of the Indian continent, a passive margin since the Paleozoic, may have had an irregular shape resulting in differential shortening strain within the Lhasa block (Plates 1 and 8a). Intense volcanic eruptions from the Gangdese arc (Plate 7a) caused deposition of the Linzizong volcanics along the southern margin of Asia largely between 60 and 50 Ma [*Pan*, 1992]. Initial contact between the Indian and Asian continents began at ~50 Ma (Plate 7a). Between 50 and 35 Ma, the thin crust of the northern Indian continent was subducted beneath the accretionary complex **(Plate 7a)**. Because the northern margin of India had relatively thin crust prior to collision, plate convergence during this period of 50 to 35 Ma may have been partially accommodated along the north dipping suture zone and produced no significant mountain belts in southernmost Tibet and northern India (Plate 7a). The rest of the convergence could have been accommodated by thrusts and strike-slip faults further to the north and east, such as the Red River ductile shear zone, during this period. In map view (Plate 8b), the proposed irregular geometry of the northeastern Indian continent would have caused, in this small region, a diachronous collision of India with Asia (i.e., collision began first to the east and propagated to the west). Further convergence between India and Asia occurred during 35 to 27 Ma along the north dipping suture and may have produced a low-elevation mountain range along the southern margin of the Asian continent. The GT first developed between 27 and 23 Ma. The style of deformation within the GTS changed along strike, perhaps as a response to the irregular geometry of the northern edge of the Indian continent (i.e., a single thrust (GT) east of Renbu, and a pop-up structure west of Renbu) (Plates 8b and 8c). During this interval, the GT east of Renbu cut through the Gangdese batholith (Plate 7e) and carried the plutonic rocks over the Xigaze forearc deposits (Plates 7f and 8c). Underthrusting of the Xigaze Group and the Tethyan sediments caused rapid cooling of rocks directly above the GT. Movement along the Gangdese thrust contributed to creation of the Gangdese range along the southern margin of the Tibetan plateau. The irregular topography of the Moho due to this crustal shortening event may have been smoothed by ductile flow in the lower crust (Plate 7f). Late in the 27-20 Ma period, the Main Central Thrust (MCT) and the North Himalayan (normal) fault (NHF) developed. The RZT that postdates the GT appears to have developed coevally with the MCT and early motion on the NHF; its hanging wall may have formed as a backthrust of the MCT and the thrust toe of the NHF accommodating the local extension strain in the Higher Himalaya (Plates 7d and 7g). Further northward thrusting along the Renbu-Zedong fault obscures the trace of the GT and the suture along which the ocean(s) between India and Asia was consumed (Plate 8e).

Conclusions

Structural and thermochronological investigations conducted in southern Tibet reveal that intracontinental thrusting has been the dominant cause for the formation of the southeastern Tibetan (Qinghai-Xizang) Plateau since the late Oligocene. Two major thrust systems are documented: the north dipping Gangdese system and the younger south dipping Renbu-Zedong thrust system. West of Renbu, the Gangdese thrust juxtaposes the Xigaze Group over the Tethyan sedimentary rocks of the Indian plate, whereas east of Lhasa, the fault juxtaposes the Gangdese batholith over Tethyan metasedimentary rocks. Near Zedong, the GT is marked by a >200-m-thick mylonitic shear zone that consists of deformed granite and metasedimentary rocks. A major south dipping backthrust in the hanging wall of the GT puts the Xigaze Group over Tertiary conglomerates or the Gangdese plutonic rocks in places. The style of deformation in the Xigaze Group is characterized by widely developed folds that are south verging directly above the GT to the south and north verging folds and north directed duplex systems above the backthrust to the north. The timing of movement on the GT is constrained to be between 27 and ~23 Ma based on $^{40}Ar/^{39}Ar$ thermochronology with a minimum displacement estimated to be 46±9 km giving a minimum slip rate along the GT of 12±6 mm/yr. The younger RZT is thrust over the trace of the GT in many localities obscuring its exposure. The age of the RZT is constrained to be between 23-8 Ma. The suture zone between India and Asia has been complexly modified by the regionally developed GT and RZT systems and locally developed left-slip and normal fault systems.

Acknowledgments. We thank Li Qi (State Seismological Bureau), Yiao Zhong-Fu (Xizang Bureau of Geology), and Barshang Tseren (Xizang Seismological Bureau) for assisting in the field, Wang Jo and Li (Niang Ci Pi) Shi-fu for their careful driving, Dave Foster for the fission-track age, Matt Heizler for assistance with the $^{40}Ar/^{39}Ar$ measurements, Mike McWilliams and an anonymous reviewer for useful suggestions to improve clarity of the manuscript and G. Lister for microscopic examination of the sense of shear indicators. We are grateful for the leadership of Zhou Xinhua, who skillfully organized the field operation. This research was supported by NSF grants EAR-9118125 and EAR-9118827, the Department of Energy, Institute of Geophysics and Planetary Physics of Lawrence Livermore National Laboratory, and the Chinese National Natural Science Foundation grant 49173161.

References

Allegre, C.J., et al., Structure and evolution of the Himalaya-Tibet orogenic belt, *Nature, 307*, 17-22, 1984.

Argand, E., La tectonique de l'Asie, *Proc. 13th Int. Geol. Congr., 7*, 171-372, 1924.

Avouac, J.P., and P. Tapponnier, Kinematic model of active deformation in central Asia, *Terra Abstr., 5*, 252-253, 1993.

Axen, G.J., Pore pressure, stress increase, and fault weakening in low angle normal faulting, *J. Geophys. Res., 97*, 8979-8991, 1992.

Bouchez, J.L. and A. Pêcher, Himalayan Main Central Thrust pile and its quartz-rich tectonites in central Nepal, *Tectonophysics, 78*, 23-50, 1981.

Burchfiel, B.C., and L.H. Royden, North-south extension within the convergent Himalayan region, *Geology, 13*, 679-682, 1985.

Burchfiel, B.C., Z. Chen, K.V. Hodges, Y. Liu, L.H. Royden, C. Deng, and J. Xu, The South Tibetan Detachment System, Himalayan orogen: Extension contemporaneous with and parallel to shortening in a collisional mountain belt, *Spec. Pap. Geol. Soc. Am. , 269*, 1-41, 1992.

Burg, J.P. (Compiler) Carte géologique du sud du Tibet, scale, 1:500,000, Cent. Natl. de la Rech. Sci., Paris, 1983.

Burg, J.P., M. Brunel, D. Gapais, G.M. Chen, and G.H. Lin, Deformation of leucogranites of the crystalline Main Central Sheet in southern Tibet (China), *J. Struct. Geol., 6*, 535-542, 1984.

Chang, C. et al., Preliminary conclusions of the Royal Society and Academia Sinica 1985 geotraverse of Tibet, *Nature, 323*, 501-507, 1986.

Copeland, P., T.M. Harrison, W.S.F. Kidd, X. Ronghua, and Z. Yuquan, Rapid early Miocene acceleration of uplift in the Gangdese Belt, Xizang-southern Tibet, and its bearing on accommodation mechanisms of the India-Asia collision, *Earth Planet. Sci. Lett., 86*, 240-252, 1987.

Copeland, P., R.R. Parrish, and T.M. Harrison, Identification of inherited radiogenic Pb in monazite and its implications for U-Pb systematics, *Nature, 333*, 760-763, 1988.

Copeland, P., T.M. Harrison, and P. LeFort, Age and cooling history of the Manaslu granite: Implications for Himalayan tectonics, *J. Volcanol. Geotherm. Res., 44*, 33-50, 1990.

Copeland, P., T.M. Harrison, K.V. Hodges, P. Maréujol, P. LeFort, and A. Pêcher, An early Pliocene thermal perturbation of the Main Central Thrust, Central Nepal: Implications for Himalayan tectonics, *J. Geophys. Res., 96*, 8475-8500, 1991.

Copeland, P., Y. Pan, T.M. Harrison, W.S.F. Kidd, M. Roden, and W. Chen, Thermal evolution of the Gangdese batholith, southern Tibet: A history of episodic unroofing, *Tectonics*, in press, 1994.

Dewey, J.F., and K. Burke, Tibetan, Variscan and Precambrian basement reactivation: Products of continental collision, *J. Geol., 81*, 683-692, 1973.

Dewey, J.F., R.M. Shackleton, C. Chang and Y. Sun, The tectonic evolution of the Tibetan Plateau, *Philos. Trans. R. Soc. London, A 327*, 379-413, 1988.

Dewey, J.F., S. Cande, and W.C. Pitman, Tectonic evolution of the India-Eurasia collision zone, *Eclogae Geol. Helv., 82*, 717-734, 1989.

England, P., and G. Houseman, Finite strain calculations of continental deformation, 2, Comparison with the India-Asia collision zone, *J. Geophys. Res., 91*, 3664-3676, 1986.

England, P., and P. Molnar, Surface uplift, uplift of rocks, and exhumation of rocks, *Geology, 18*, 1173-1177, 1990.

England, P., and M. Searle, The Cretaceous-Tertiary deformation of the Lhasa block and its implications for crustal thickening in Tibet, *Tectonics, 5*, 1-14, 1986.

Fitz Gerald, J.D., and T.M. Harrison, Argon diffusion domains in K-feldspar, I; Microstructures in MH-10, *Contrib. Mineral. Petrol., 113*, 367-380, 1993.

Gansser, A., The geodynamic history of the Himalaya, in *Zagros, Hindu Kush, Himalaya-Geodynamic Evolution*, Geodynamic Ser., vol. 3, edited by H.K. Gupta and F.M. Delany, pp. 111-121, AGU, Washington, D. C., 1981.

Green, P.F., On the thermo-tectonic evolution of Northern England: Evidence from fission track dating, *Geol. Mag., 123*, 493-506, 1986.

Harrison, T.M., I. Duncan, and I. McDougall, Diffusion of ^{40}Ar in biotite: Temperature, pressure and composition effects, *Geochim. Cosmochim. Acta, 49*, 2461-2468, 1985.

Harrison, T.M., O.M. Lovera and M.T. Heizler, $^{40}Ar/^{39}Ar$ results for multi-domain samples with varying activation energy. *Geochim. Cosmochim. Acta, 55*, 1435-1448, 1991.

Harrison, T.M., P. Copeland, W.S.F. Kidd, and A. Yin, Raising Tibet, *Science, 255*, 1663-1670, 1992a.

Harrison, T.M., W. Chen, P.H. Leloup, F.J. Ryerson, and P. Tapponnier, An early Miocene transition in deformation regime within the Red River fault zone, Yunnan, and its significance for Indo-Asian tectonics, *J. Geophys. Res., 97*, 7159-7182, 1992b.

Harrison, T.M., P. Copeland, S. Hall, J. Quade, S. Burner, T.P. Ojha, and W.S.F. Kidd, Isotopic preservation of Himalayan/Tibetan uplift, denudation, and climatic histories in two molasse deposits, *J. Geol., 101*, 159-177, 1993a.

Harrison, T.M., M.T. Heizler, and O.M. Lovera, In vacuo crushing experiments and K-feldspar thermochronometry, *Earth Planet. Sci. Lett., 117*, 169-180, 1993b.

Hodges, K., B.C. Burchfiel, Z. Chen, T. Housh, D. Lux, R. Parrish, and L.H. Royden, Rapid early Miocene tectonic unroofing of the metamorphic core of the Himalaya: Evidence from the Qomolangma (Everest) region, Tibet, *Geol. Soc. Am. Abstr. Programs, 23*, 372, 1991.

Honegger, K., V. Dietrich, W. Frank, A. Gansser, M. Thöni, and V. Trommsdorff, Magmatism and metamorphism in the Ladakh Himalayas (the Indus-Tsangpo suture zone), *Earth Planet. Sci. Lett., 60*, 253-292, 1982.

Hubbard, M.S., and T.M. Harrison, $^{40}Ar/^{39}Ar$ age constraints on deformation and metamorphism in the MCT Zone and Tibetan Slab, eastern Nepal Himalaya, *Tectonics, 8*, 865-880, 1989.

Kidd, W.S.F., Y. Pan, C. Chang, M.P. Coward, J.F. Dewey, A. Gansser, P. Molnar, R.M. Shackleton, and Y. Sun, Geological mapping of the 1985 Chinese-British (Xizang-Qinghai) Geotraverse route, *Philos. Trans., R. Soc. London, Ser. A, 327*, 287-305, 1988.

LeFort, P., Metamorphism and magmatism during the Himalayan collision, in Collision Tectonics, edited by M.P. Coward and A.C. Ries, *Geol. Soc. Spec. Publ. London, 19*, 159-172, 1986.

Leloup, P.H., T.M. Harrison, F.J. Ryerson, W. Chen, Q. Li, P. Tapponnier, and R. Lacassin, Structural, petrological and thermal evolution of a Tertiary ductile strike-slip shear zone, Diancang Shan, Yunnan, *J. Geophys. Res., 98*, 6715-6743, 1993.

Le Pichon, X., M. Fournier, and L. Jolivet, Kinematics, topography, shortening, and extrusion in the India-Eurasia collision, *Tectonics, 11*, 1085-1098, 1992.

Liu, Z.Q., et al., Geologic Map of Qinghai-Xizang Plateau and its Neighboring Regions (in Chinese), scale, 1:500,000, Chengdu Inst. Geol. and Min. Resour., Acad. Sini., Geol. Publisher, Beijing, 1988.

Lovera, O.M., F.M. Richter, and T.M. Harrison, $^{40}Ar/^{39}Ar$ geothermometry for slowly cooled samples having a distribution of diffusion domain sizes, *J. Geophys. Res., 94*, 17,917-17,935, 1989.

Lovera, O.M., F.M. Richter, and T.M. Harrison, Diffusion domains determined by ^{39}Ar release during step heating, *J. Geophys. Res., 96*, 2057-2069, 1991.

Lovera, O.M., M.T. Heizler, and T.M. Harrison, Argon diffusion domains in K-feldspar, II; Kinetic properties of MH-10, *Contrib. Mineral. Petrol., 113*, 381-393, 1993.

Lyon-Caen, H., and P. Molnar, Constraints on the structure of the Himalaya from an analysis of gravity anomolies and a flextural model of the lithosphere, *J. Geophys. Res., 88*, 8171-8191, 1983.

Lyon-Caen, H., and P. Molnar, Gravity anomalies, flexure of the Indian plate, and the structure, support and evolution of the Himalaya and Ganga Basin, *Tectonics, 4*, 513-538, 1985.

Maluski, H., P. Matte, and M. Brunel, Argon 39-Argon 40 dating of metamorphic and plutonic events in the North and High Himalayas belts (southern Tibet-China), *Tectonics, 7*, 299-326, 1988.

Mattauer, M., Intracontinental subduction, crustal stacking wedge and crust-mantle decollement, in Collision Tectonics, edited by M.P. Coward and A.C. Ries, *Geol. Soc. Spec. Publ. London, 19*, 35-60, 1986.

McDougall, I., and T.M. Harrison, *Geochronology and Thermochronology by the $^{40}Ar/^{39}Ar$ Method*, 212 pp., Oxford University Press, New York, 1988.

Molnar, P., and Q. Deng, Faulting associated with large earthquakes and the average rate of deformation in Central and Eastern Asia, *J. Geophys. Res., 89*, 6203-6227, 1984.

Pan, Y., Unroofing history and structural evolution of the southern Lhasa Terrane, Tibetan Plateau: Implications for the continental collision between India and Asia, Ph.D. thesis, 395 pp., State Univ. of N. Y. at Albany, 1992.

Pan, Y., and W.S.F. Kidd, Nyainqentanglha shear zone: A late Miocene extensional detachment in the southern Tibetan Plateau, *Geology, 20*, 775-778, 1992.

Parrish, R.R., U-Pb dating of monazite and its application to geological problems, *Can. J. Earth Sci., 27*, 1426-1431, 1990.

Parrish, R.R., and K.V. Hodges, Miocene (22±1) metamorphism and two stage thrusting in the Greater Himalayan sequence, Annapurna Sanctuary, Nepal, *Geol. Soc. Am. Abstr. Programs, 25*, A174, 1993.

Pêcher, A., The contact between the higher Himalayan cystallines and the Tibetan sedimentary series: Miocene large-scale dextral shearing, *Tectonics, 10*, 587-598, 1991.

Peltzer, G., and P. Tapponnier, Formation and evolution of strike-slip faults, rifts, and basins during the India-Asia collision: An experimental approach, *J. Geophys. Res., 93*, 15,085-15,117, 1988.

Powell, C. M., and P.G. Conaghan, Plate tectonics and the Himalayas, *Earth Planet. Sci. Lett., 81*, 1431-1450, 1973.

Richter, F.M., O.M. Lovera, T.M. Harrison, and P. Copeland, Tibetan tectonics from a single feldspar sample: An application of the $^{40}Ar/^{39}Ar$ method, *Earth Planet. Sci. Lett., 105*, 266-276, 1991.

Richter, F.M., D.B. Rowley, and D.J. DePaolo, Sr isotope evolution of seawater: The role of tectonics, *Earth Planet. Sci. Lett., 109*, 11-23, 1992.

Schärer, U., The effect of initial ^{230}Th disequilibrium on young U-Pb ages: The Makalu case, Himalaya, *Earth Planet. Sci. Lett., 67*, 191-204, 1984.

Schärer, U., R. Xu, and C. Allegre, U-Pb geochronology of Gangdese (Transhimalayan) plutonism in the Lhasa-Xigaze region, Tibet, *Earth Planet. Sci. Lett., 69*, 311-320, 1984.

Schärer, U., R. Xu, and C. Allegre, U-(Th)-Pb systematics and ages of Himalayan leucogranites, south Tibet, *Earth Planet. Sci. Lett., 77*, 35-48, 1986.

Searle, M.P., et al., The closing of Tethys and the tectonics of the Himalaya, *Geol. Soc. Am. Bull, 98*, 678-701, 1987.

Shi, Y., and C.Y. Wang, Two-dimensional modeling of the P-T-t paths of regional metamorphism in simple overthrust terrains, *Geology, 15*, 1048-1051, 1987.

Tapponnier, P., G. Pelltzer, A.Y. Le Dain, R. Armijo, and P. Cobbold, Propagating extrusion tectonics in Asia: New insight from simple experiments with plasticine, *Geology, 10*, 1339-1384, 1982.

Wang, X., Z. M. Li, and Qiangba-Xiyiao, Geologic Map of the Xigaze-Zedong Region (in Chinese), scale, 1:100,000, Xizang (Tibet) with report, 568 pp., Xizang Bur. Geol., Lhasa, 1983.

Yin, A., Mechanics of wedge-shaped fault blocks, I; An elastic solution for compressional wedges, *J. Geophys. Res., 98*, 14,245-14,256, 1993.

Chen W., Institute of Geology, State Seismological Bureau, Beijing 100029, People's Republic of China.

P. Copeland, Department of Geosciences, University of Houston, Houston, Texas 77204-5503.

T. M. Harrison and A. Yin, Department of Earth and Space Sciences and Institute of Geophysics and Planetary Physics, University of California, Los Angeles, CA 90024-1567.

W. S. F. Kidd, Department of Geological Sciences, State University of New York at Albany, Albany, NY 12222.

F. J. Ryerson, Institute of Geophysics and Planetary Physics, Lawrence Livermore National Laboratory, Livermore, CA 94550.

(Received April 26, 1993; revised December 6, 1993; accepted February 15, 1994.)